Contemporary Mathematics
https://ojs.wiserpub.com/index.php/CM/

Research Article

Complex Dynamical Analysis of a Discretized Fractional Order Tumor Dormancy Model with Chaotic Behavior

Fuat Gurcan[1*], Norah Alqenaei[1], Senol Kartal[2]

[1]Department of Mathematics, College of Science, Kuwait University, Sabah Al Salem University City, P.O. Box 5969, Safat, 13060, Shadadiya
[2]Department of Science and Mathematics Education, Faculty of Education, Nevsehir Haci Bektas Veli University, Nevsehir, 50300, Turkey
E-mail: fuat.gurcan@ku.edu.kw

Received: 14 October 2025; **Revised:** 13 January 2026; **Accepted:** 13 January 2026

Abstract: A discrete fractional order model of tumor-immune interaction is proposed to investigate cancer dormancy. The investigation shows that the model undergoes a Neimark-Sacker bifurcation, leading to chaos. The classical predator-prey model is typically used to describe interactions between two biological populations, and it is adapted here to reflect the complex relationship between tumor cells and lymphocytes. Building on earlier continuous models that use fractional calculus to capture memory effects and long-term immune responses, a discrete version of a continuous fractional order model is constructed using piecewise constant arguments, where the continuous time t is divided into equal intervals of length h and replaced by $h[\frac{t}{h}]$. The function's value is taken at the start of each interval and held constant until the next one. Then, the stability of the fixed points is analyzed, and the exact conditions under which they exist and remain stable are clearly identified. Using bifurcation theory and center manifold theory, a Neimark-Sacker bifurcation at the positive fixed point is verified under certain parameter conditions. In the feedback control section, control terms are added to reduce tumor growth and stabilize the chaotic behavior of the system. Numerical simulations are then used to show the accuracy of the analytical results. Furthermore, the behavior of the system is investigated as the parameters r, σ, and α vary. At $\sigma^* = 0.432277$, the system undergoes a Neimark-Sacker, and the Lyapunov exponent is positive for $\sigma < 0.432277$ for certain parameter values, confirming the occurrence of chaos. Finally, the impact of varying the fractional order α on the system's stability is examined.

Keywords: tumor dormancy, fractional order, Caputo fractional derivative, piecewise constant arguments, stability, Neimark-Sacker bifurcation, chaos

MSC: 34A08, 37G15, 39A28, 39A33

1. Introduction

Cancer is one of the most common and difficult diseases to treat due to its complex nature. As a result, understanding cancer dynamics requires understanding how the past behavior of the system affects its current behavior, which highlights the importance of memory effects in modeling biological systems. Since classical differential equations have no memory

DOI: https://doi.org/10.37256/cm.7120268851

effect, the fractional differential equation is required in this case, which generalizes the concept of differentiation to non-integer orders.

In this paper, we consider the discrete version of a fractional tumor-immune model with dormancy proposed by Silva et al. [1], based on the Caputo fractional derivative, which accounts for memory effects. Their work represents a generalization of the classical model originally proposed by Sotolongo-Costa et al. [2], who reformulated the classical predator-prey model to describe the interaction between lymphocytes (predators) and tumor cells (prey). They also introduced additional terms to describe actions such as lymphocyte death due to an increased tumor cell population and lymphocyte flow to the interaction site between the populations. These modifications were introduced to reproduce key features of tumor behavior, including short-term oscillations in tumor size and long-term tumor relapse, as well as to account for tumor aggressiveness, lymphocyte diffusion, and the effects of cytokines on the tumor. Silva et al. [1] studied the model both mathematically and biologically, demonstrating how the use of a fractional derivative can alter the behavior of cancer dormancy and thereby provide a deeper understanding of the system. They also pointed out that the fractional version of this model enables the exploration of new scenarios to investigate cancer dormancy and provides a more in-depth analysis of its dynamics [1].

The fractional version of the nondimensional model introduced by Silva et al. [1] is given by

$$\begin{aligned} D^{\alpha}N(t) &= rN - NI, \\ D^{\alpha}I(t) &= \sigma - \frac{1}{r}I - dN + NI, \end{aligned} \tag{1}$$

where D^{α} is the Caputo fractional derivative of order $\alpha \in (0, 1)$ defined for $t > 0$ by [1, 3]

$$D^{\alpha}_{t_0} f(t) = \frac{1}{\Gamma(m-\alpha)} \int_{t_0}^{t} (t-s)^{m-\alpha-1} \frac{d^m}{ds^m} f(s)\, ds,$$

where m is a natural number, Γ is the Euler's Gamma function, $m-1 < \mathrm{Re}(\alpha) \leq \alpha$, and $N(0) = N_0$, $I(0) = I_0$, see Appendix A.1 for the derivation steps of the nondimensional model (1).

Recent studies have used different definitions of fractional derivatives in modeling dynamical systems. He's derivative has been applied to an exothermic reactions model with constant heat source in porous media [4], the local fractional derivative has been applied to a low-pass electrical transmission lines model [5], and the Caputo fractional derivative has been applied to a model of Human Immunodeficiency Virus (HIV) [6], etc. Among different definitions of fractional derivatives, the Caputo fractional derivative is the most suitable one for modeling biological systems. As it allows standard initial conditions to be applied and provides results that are very close to those of the classical derivative, especially for a constant function, for which the Caputo derivative equals zero [7]. Physically, since the biological systems have a memory effect, the Caputo derivative shows that the current rates of change of the tumor and immune populations do not depend only on the current state but also depend on their previous interactions.

For model (1), $N(t)$ represents the population of tumor cells, and $I(t)$ represents the population of lymphocytes. The nondimensional parameters in model (1) have clear biological interpretations: the parameter r indicates the growth rate of tumor cells in exponential form, where the growth rate of a tumor is proportional to the tumor burden. The parameter σ represents the lymphocyte flow constant to the interaction site between the populations and is a critical indicator in a tumor dormancy model. High σ leads to suppression of tumor cell proliferation and maintenance of the tumor in a dormant state, whereas low σ leads the immune system to escape immune surveillance and exit dormancy. The parameter d describes the death rate of lymphocytes due to an increase in tumor cells. The interaction between the two populations is denoted by NI, and it reflects negative effects on tumor cells and positive effects on lymphocytes [1, 2].

System (1), considered in [1, 2], is a two-dimensional continuous-time dynamical system and exhibits different dynamical behaviors such as a stable equilibrium point, damped oscillatory, and periodic oscillatory with constant amplitude (limit cycle). However, it is insufficient for capturing certain dynamic behaviors present in cancer dynamics, such as chaos, because according to the Poincaré-Bendixson theorem, deterministic chaos can only occur in continuous systems with three or more dimensions [8]. Therefore, the originality of this paper is that we consider the discrete version of a fractional tumor-immune model (1), which overcomes this limitation.

A better understanding of cancer mechanisms depends on examining the chaotic behavior of cancer cells. Incorporating chaotic dynamics into tumor modeling enhances the biological realism of the models and provides a framework to help explain nonlinear, unpredictable, and heterogeneous tumor behaviors. In clinical observations, sometimes the tumor may suddenly become aggressive while following a stable course or may grow rapidly and metastasize. These clinical observations may help explain unpredictable behavior such as chaos in tumor-immune dynamics. The most direct way to investigate chaos in two dimensions is to resort to a discrete-time system, which exhibits richer dynamic behaviors compared to continuous-time dynamical systems [9–11].

Gurcan et al. [12], and Kartal [13] demonstrate that bifurcations and chaotic behaviors can arise in discretized fractional order predator-prey and duopoly models due to fractional memory effects. In Gurcan et al. [12], the tumor-immune model is extended from the classical Lotka-Volterra model by incorporating immune stimulation, nonlinear immune suppression, and a constant immune source term. Neimark-Sacker bifurcations are observed in their study, whereas Kartal [13] reports the emergence of chaos through a flip bifurcation. The current study shows that similar complex behavior can occur in a discretized tumor dormancy model.

The present paper aims to capture tumor-immune dynamics more realistically by incorporating fractional order operators and a discrete-time system, which can produce complex dynamical behavior such as chaos. By integrating fractional order dynamics into a discrete-time framework, our study provides a more realistic representation of tumor-immune interactions, offering new theoretical insights and potential implications that may help in understanding cancer progression.

The paper is organized in the following way: Section 2 introduces the construction of a discrete dynamical system via a discretization approach based on piecewise constant arguments. In section 3, the stability of the fixed points is analyzed using eigenvalue analysis, center manifold theory, the Jury test, and the Schur-Cohn criterion. In section 4, it is shown that model (3) exhibits a Neimark-Sacker bifurcation around the positive fixed point. In section 5, we introduce a feedback control method to stabilize chaotic behavior at the unstable fixed point. In section 6, we present a numerical simulation to support the theoretical analysis. Section 7 provides a short conclusion.

2. Discretization process

Much research has shown that discrete systems are useful for studying cancer growth, aging, cell proliferation, and genetics, as they are more efficient in numerical simulations and can show rich and complex dynamical behaviors [14]. Discretization is an essential process that transforms a continuous-time dynamical system into a discrete system. Several techniques can be used to discretize a continuous system, like the Euler method [15]. In this paper, we consider the piecewise constant arguments method, a discretization method that was introduced to discretize the fractional order differential equations [16]. The method is used to approximate continuous-time dynamical systems by holding certain variables constant over discrete intervals. A key reason for using this method is that the discretization yields important parameters such as the time step h and the fractional order α [17]. The parameter α plays an important role in controlling how strong the memory effect is. Following earlier works [16, 18], we consider model (1) with piecewise constant arguments as follows:

$$
\begin{aligned}
D^{\alpha}N(t) &= rN\left(h[\frac{t}{h}]\right) - N\left(h[\frac{t}{h}]\right) I\left(h[\frac{t}{h}]\right), \\
D^{\alpha}I(t) &= \sigma - \frac{1}{r} I\left(h[\frac{t}{h}]\right) - dN\left(h[\frac{t}{h}]\right) + N\left(h[\frac{t}{h}]\right) I\left(h[\frac{t}{h}]\right),
\end{aligned} \tag{2}
$$

where $h\left[\frac{t}{h}\right]$ is the piecewise constant argument, $\left[\frac{t}{h}\right]$ is the greatest integer less than or equal to $\frac{t}{h}$, and $h > 0$ is the discretization parameter. The initial conditions are $N(0) = N_0$, $I(0) = I_0$.

Let $t \in [0, h)$, then $\frac{t}{h} \in [0, 1)$. So, we get

$$D^{\alpha}N(t) = rN_0 - N_0I_0,$$

$$D^{\alpha}I(t) = \sigma - \frac{1}{r}I_0 - dN_0 + N_0I_0,$$

using the fractional integral of order α defined by

$$I^{\alpha}f(t) = \int_0^t \frac{(t-s)^{\alpha-1}}{\Gamma(\alpha)} f(s)\, ds$$

on both sides of the previews system, we obtain

$$I^{\alpha}D^{\alpha}N(t) = I^{\alpha}(rN_0 - N_0I_0),$$

$$I^{\alpha}D^{\alpha}I(t) = I^{\alpha}(\sigma - \frac{1}{r}I_0 - dN_0 + N_0I_0),$$

which gives

$$N_1(t) - N_0 = I^{\alpha}(rN_0 - N_0I_0),$$

$$I_1(t) - I_0 = I^{\alpha}(\sigma - \frac{1}{r}I_0 - dN_0 + N_0I_0),$$

where

$$I^{\alpha}(rN_0 - N_0I_0) = \int_0^t \frac{(t-s)^{\alpha-1}}{\Gamma(\alpha)} (rN_0 - N_0I_0)\, ds$$

$$= \frac{(rN_0 - N_0I_0)}{\Gamma(\alpha)} \int_0^t (t-s)^{\alpha-1}\, ds$$

$$=\frac{(rN_0 - N_0I_0)}{\Gamma(1+\alpha)}t^{\alpha}.$$

Similarly, we obtain

$$I^{\alpha}(\sigma - \frac{1}{r}I_0 - dN_0 + N_0I_0) = \frac{(\sigma - \frac{1}{r}I_0 - dN_0 + N_0I_0)}{\Gamma(1+\alpha)}t^{\alpha},$$

and the solution of (2) is given by

$$N_1(t) = N_0 + \frac{t^{\alpha}}{\Gamma(1+\alpha)}\left(rN_0 - N_0I_0\right),$$

$$I_1(t) = I_0 + \frac{t^{\alpha}}{\Gamma(1+\alpha)}\left(\sigma - \frac{1}{r}I_0 - dN_0 + N_0I_0\right).$$

Applying the same process for $t \in [h, 2h)$. Then, we obtain

$$D^{\alpha}N(t) = rN_1(h) - N_1(h)I_1(h),$$

$$D^{\alpha}I(t) \ = \sigma - \frac{1}{r}I_1(h) - dN_1(h) + N_1(h)I_1(h),$$

which gives

$$N_2(t) = N_1(h) + I^{\alpha}(rN_1(h) - N_1(h)I_1(h)),$$

$$I_2(t) = I_1(h) + I^{\alpha}(\sigma - \frac{1}{r}I_1(h) - dN_1(h) + N_1(h)I_1(h)),$$

where

$$I^{\alpha}(rN_1(h) - N_1(h)I_1(h)) = \int_h^t \frac{(t-s)^{\alpha-1}}{\Gamma(\alpha)}(rN_1(h) - N_1(h)I_1(h))\,ds$$

$$=\frac{(rN_1(h) - N_1(h)I_1(h))}{\Gamma(\alpha)}\int_h^t (t-s)^{\alpha-1}\,ds$$

$$=\frac{(rN_1(h) - N_1(h)I_1(h))}{\Gamma(1+\alpha)}(t-h)^{\alpha}.$$

Similarly, we obtain

$$I^{\alpha}(\sigma-\frac{1}{r}I_1(h)-dN_1(h)+N_1(h)I_1(h))=\frac{(\sigma-\frac{1}{r}I_1(h)-dN_1(h)+N_1(h)I_1(h))}{\Gamma(1+\alpha)}(t-h)^{\alpha}.$$

Therefore, the solution of system (2) is given by

$$N_2(t)=N_1(h)+\frac{(t-h)^{\alpha}}{\Gamma(1+\alpha)}\left(rN_1(h)-N_1(h)I_1(h)\right),$$

$$I_2(t)=I_1(h)+\frac{(t-h)^{\alpha}}{\Gamma(1+\alpha)}\left(\sigma-\frac{1}{r}I_1(h)-dN_1(h)+N_1(h)I_1(h)\right).$$

Repeating the process, we get that when $t\in[nh,\,(n+1)h)$, then $\frac{t}{h}\in[n,\,n+1)$. So, we have

$$D^{\alpha}N(t)=rN_n(nh)-N_n(nh)I_n(nh),$$

$$D^{\alpha}I(t)\ =\sigma-\frac{1}{r}I_n(nh)-dN_n(nh)+N_n(nh)I_n(nh),$$

and the solution of (2) is given by

$$N_{n+1}(t)=N_n(nh)+\frac{(t-nh)^{\alpha}}{\Gamma(1+\alpha)}\left(rN_n(nh)-N_n(nh)I_n(nh)\right),$$

$$I_{n+1}(t)=I_n(nh)+\frac{(t-nh)^{\alpha}}{\Gamma(1+\alpha)}\left(\sigma-\frac{1}{r}I_n(nh)-dN_n(nh)+N_n(nh)I_n(nh)\right).$$

By letting $t\to(n+1)h$, we obtain the discretization

$$N_{n+1}((n+1)h)=N_n(nh)+\frac{h^{\alpha}}{\Gamma(1+\alpha)}\left(rN_n(nh)-N_n(nh)I_n(nh)\right),$$

$$I_{n+1}((n+1)h)=I_n(nh)+\frac{h^{\alpha}}{\Gamma(1+\alpha)}\left(\sigma-\frac{1}{r}I_n(nh)-dN_n(nh)+N_n(nh)I_n(nh)\right),$$

which can be rewritten as

$$\begin{cases} N_{n+1}=N_n+\dfrac{h^{\alpha}}{\Gamma(1+\alpha)}\left(rN_n-N_nI_n\right), \\ \\ I_{n+1}\ =I_n+\dfrac{h^{\alpha}}{\Gamma(1+\alpha)}\left(\sigma-\dfrac{1}{r}I_n-dN_n+N_nI_n\right), \end{cases} \tag{3}$$

where $n \geq 0$ (integer), and as $\alpha \to 1$ in model (3), $\lim_{\alpha\to 1} \dfrac{h^\alpha}{\Gamma(1+\alpha)} = h$. Hence, the Euler discretization method of Chua's system is obtained [15].

3. Existence and stability of fixed (equilibrium) points

A fixed point is a solution that stays unchanged as time progresses. In tumor-immune interaction models, the stability of a fixed point determines whether the system returns to equilibrium or continues to move away after small disturbances. Biologically, a stable tumor-free equilibrium means that small numbers of tumor cells are eliminated by the immune system, while a stable coexistence equilibrium reflects tumor dormancy, where the tumor is controlled but persists under immune surveillance. Conversely, the instability of these equilibria indicates that minor changes can lead to tumor growth.

Now, mathematically it is easy to see that both systems (1) and (3) exhibit the same set of fixed points: $E_0 = (0, r\sigma)$, and $E_1 = (N^*, I^*) = \left(\dfrac{1-\sigma}{r-d}, r\right)$ for $r \neq d$. E_0 is the tumor-free (exclusion) fixed point, and E_1 is the coexistence fixed point. We note that E_1 is positive under the condition $r < d$ and $\sigma > 1$, or $r > d$ and $\sigma < 1$. Therefore, E_1 is identified as the only positive fixed point of system (3). Throughout model (3), the parameters r, d, σ, and h are assumed to be positive, with $\alpha \in (0, 1)$.

3.1 *Stability analysis of the first fixed point E_0*

Lemma 1 For the tumor-lymphocyte system (3), and if $r > \dfrac{h^\alpha}{2\Gamma(1+\alpha)}$, the following results hold true for the fixed point $E_0 = (0, r\sigma)$.

(i) If $1 < \sigma < 1 + \frac{2\Gamma(1+\alpha)}{rh^\alpha}$, then E_0 is asymptotically stable.

(ii) If $\sigma < 1$ or $\sigma > 1 + \frac{2\Gamma(1+\alpha)}{rh^\alpha}$, then E_0 is a saddle point.

(iii) If $\sigma = 1$, then E_0 is nonhyperbolic and it satisfies:

- If $r = d$, it is stable but not asymptotically stable.
- If $r \neq d$, it is unstable (semistable).

Proof. (i) The Jacobian matrix of system (3) can be calculated as

$$J = \begin{pmatrix} \dfrac{h^\alpha(r-I)}{\Gamma(1+\alpha)} + 1 & -\dfrac{Nh^\alpha}{\Gamma(1+\alpha)} \\ \dfrac{(I-d)h^\alpha}{\Gamma(1+\alpha)} & \dfrac{h^\alpha}{\Gamma(1+\alpha)}\left(N - \dfrac{1}{r}\right) + 1 \end{pmatrix}. \tag{4}$$

Evaluating the Jacobian matrix J of system (3) at the fixed point $(0, r\sigma)$, we get

$$J(0, r\sigma) = \begin{pmatrix} \dfrac{h^\alpha(r-r\sigma)}{\Gamma(1+\alpha)} + 1 & 0 \\ \dfrac{h^\alpha(r\sigma-d)}{\Gamma(1+\alpha)} & 1 - \dfrac{h^\alpha}{r\Gamma(1+\alpha)} \end{pmatrix}. \tag{5}$$

Since the Jacobian matrix (5) is triangular matrix, its eigenvalues are

$$\lambda_1 = 1 + \frac{r(1-\sigma)h^\alpha}{\Gamma(1+\alpha)}, \text{ and } \lambda_2 = 1 - \frac{h^\alpha}{r\Gamma(1+\alpha)}.$$

The condition $|\lambda_1| < 1$ leads to $1 < \sigma < 1 + \frac{2\Gamma(1+\alpha)}{rh^\alpha}$, and the condition $|\lambda_2| < 1$ leads to $r > \frac{h^\alpha}{2\Gamma(1+\alpha)}$. Hence, the proof is complete.

(ii) $|\lambda_2| < 1$ leads to the condition $r > \frac{h^\alpha}{2\Gamma(1+\alpha)}$, and $|\lambda_1| > 1$ if either $\lambda_1 > 1$ or $\lambda_1 < -1$. If $\lambda_1 > 1$, then this leads to the condition $\sigma < 1$. If $\lambda_1 < -1$, then it leads to the condition $\sigma > 1 + \frac{2\Gamma(1+\alpha)}{rh^\alpha}$. Since $|\lambda_1| > 1$ and $|\lambda_2| < 1$, the fixed point E_0 is a saddle.

(iii) For $\sigma = 1$, we have $|\lambda_1| = 1$, which implies that the fixed point E_0 is nonhyperbolic. Hence, the stability can be determined using center manifold theory.

Letting $u = N$ and $v = I - r\sigma$ in (3), we have

$$\begin{pmatrix} u \\ v \end{pmatrix} \to \begin{pmatrix} u + \frac{h^\alpha}{\Gamma(1+\alpha)}(ru - uv - ru\sigma) \\ \\ v + \frac{h^\alpha}{\Gamma(1+\alpha)}\left(-\frac{1}{r}v - du + uv + ru\sigma\right) \end{pmatrix}. \tag{6}$$

Now, for $\sigma = 1$ and $r > \frac{h^\alpha}{2\Gamma(1+\alpha)}$, system (6) becomes

$$\begin{pmatrix} u \\ v \end{pmatrix} \to \begin{pmatrix} 1 & 0 \\ \\ \frac{(r-d)h^\alpha}{\Gamma(1+\alpha)} & 1 - \frac{h^\alpha}{r\Gamma(1+\alpha)} \end{pmatrix} \begin{pmatrix} u \\ v \end{pmatrix} + \frac{h^\alpha}{\Gamma(1+\alpha)} \begin{pmatrix} -uv \\ \\ uv \end{pmatrix}. \tag{7}$$

Let

$$D = \begin{pmatrix} 1 & 0 \\ \\ \frac{(r-d)h^\alpha}{\Gamma(1+\alpha)} & 1 - \frac{h^\alpha}{r\Gamma(1+\alpha)}, \end{pmatrix}.$$

Since the Jacobian matrix D is a triangular matrix, its eigenvalues are

$$\lambda_3 = 1 \text{ and } \lambda_4 = 1 - \frac{h^\alpha}{r\Gamma(1+\alpha)},$$

and the eigenvectors associated with λ_3 and λ_4 are

$$\begin{pmatrix} 1 \\ \\ r(r-d) \end{pmatrix} \text{ and } \begin{pmatrix} 0 \\ \\ 1 \end{pmatrix},$$

respectively.

Let T be the transformation matrix formed by the previous two eigenvectors, which transforms the Jacobian matrix D into its Jordan canonical form [19, 20],

$$T = \begin{pmatrix} 1 & 0 \\ \\ r(r-d) & 1 \end{pmatrix}.$$

By applying the translation $\begin{pmatrix} u \\ v \end{pmatrix} = T \begin{pmatrix} X \\ Y \end{pmatrix}$, map (7) can be express as

$$\begin{pmatrix} X \\ Y \end{pmatrix} \to \begin{pmatrix} 1 & 0 \\ \\ 0 & 1 - \dfrac{h^\alpha}{r\Gamma(1+\alpha)} \end{pmatrix} \begin{pmatrix} X \\ Y \end{pmatrix} + \frac{h^\alpha}{\Gamma(1+\alpha)} \begin{pmatrix} f(X,Y) \\ \\ g(X,Y) \end{pmatrix},$$

where

$$f(X,Y) = -rX^2(r-d) - XY,$$

$$g(X,Y) = rX^2(r-d)\left(-dr+r^2+1\right) + XY\left(-dr+r^2+1\right).$$

We assume that the center manifold takes the form $Y = h(X) = \beta X^2 + \gamma X^3 + \mathcal{O}(|X|^4)$. Hence, the following equation must hold

$$h(X + \frac{h^\alpha}{\Gamma(1+\alpha)} f(X, h(X)) = \left(1 - \frac{h^\alpha}{r\Gamma(1+\alpha)}\right) h(X) + \frac{h^\alpha}{\Gamma(1+\alpha)} g(X, h(X)).$$

Based on estimates, the center manifold leads to $\beta = r(r^2 - rd)\left(-dr + r^2 + 1\right)$ and $\gamma = r^2(r^2 - rd)(1 - rd + r^2)(3r^2 - 3rd + 1)$ (see Appendix A.2 for computation details).

Thus,

$$\begin{aligned} Y =& h(X) \\ =& r(r^2 - rd)\left(-dr + r^2 + 1\right)X^2 + H.O.T. \end{aligned}$$

It follows that a one dimensional map $\hat{f}$ can be expressed as

$$\hat{f} = X + \frac{h^\alpha}{\Gamma(1+\alpha)}\left((rd-r^2)X^2 - r(r^2-rd)(1-rd+r^2)X^3\right).$$

Now, $\hat{f}'(0) = 1$ and $\hat{f}''(0) = \frac{2h^\alpha}{\Gamma(1+\alpha)}(rd-r^2)$. Then, we examine the stability of $x^* = 0$ in the reduced map $\hat{f}$ by considering two cases for the parameters r and d.

Case 1: $r = d$

If $r = d$ then $h(X) = 0$ and therefore $\hat{f} = X$. Consequently, $\hat{f}'(0) = 1$ and $\hat{f}^{(k)}(0) = 0$ for all $k > 1$. By the Remark in Appendix A of [21], $x^* = 0$ is stable but not asymptotically stable. As a result, the original fixed point $(0, r\sigma)$ of the system inherits this stability behavior.

Case 2: $r \neq d$

If $r \neq d$, then $\hat{f}'(0) = 1$ and $\hat{f}''(0) = \frac{2h^\alpha}{\Gamma(1+\alpha)}(rd-r^2) \neq 0$. According to Theorem 1.5 in [22], $x^* = 0$ is unstable (semi-stable); more precisely,

- If $\hat{f}''(0) < 0$, then $x^* = 0$ is semi-stable from the right.
- If $\hat{f}''(0) > 0$, then $x^* = 0$ is semi-stable from the left.

As a result, the original fixed point $(0, r\sigma)$ of the system inherits this stability behavior. □

3.2 *Stability analysis of the second fixed point E_1*

For the second fixed point $E_1 = \left(\frac{1-\sigma}{r-d}, r\right)$, the Jacobian matrix (4) of system (3) is given by

$$J\left(\frac{1-\sigma}{r-d}, r\right) = \begin{pmatrix} 1 & -\frac{(1-\sigma)h^\alpha}{\Gamma(1+\alpha)(r-d)} \\ \frac{(r-d)h^\alpha}{\Gamma(1+\alpha)} & \frac{h^\alpha}{\Gamma(1+\alpha)}\left(\frac{1-\sigma}{r-d} - \frac{1}{r}\right) + 1 \end{pmatrix}. \tag{8}$$

The characteristic equation of the Jacobian matrix $J\left(\frac{1-\sigma}{r-d}, r\right)$ is given by:

$$p(\lambda) = \lambda^2 + p_1\lambda + p_0 = 0, \tag{9}$$

where

$$p_1 = \frac{h^\alpha(d-r\sigma)}{r\Gamma(1+\alpha)(d-r)} - 2, \tag{10}$$

and

$$p_0 = \frac{h^\alpha\left(\frac{\Gamma(1+\alpha)(r\sigma-d)}{r(d-r)} - (\sigma-1)h^\alpha\right)}{\Gamma(1+\alpha)^2} + 1. \tag{11}$$

According to the Jury test [23], the necessary conditions for all the roots of $p(\lambda)=0$ to satisfy $|\lambda|<1$ are: $p(1)>0$, $p(-1)>0$, and $|p_0|<1$.

Lemma 2 For the tumor-lymphocyte system (3), if $r<d$ and $\sigma>1$, the fixed point $\left(\frac{1-\sigma}{r-d}, r\right)$ is unstable.

Proof. Under the condition $r<d$ and $\sigma>1$, and from (9), we have

$$p(1)=-\frac{(\sigma-1)h^{2\alpha}}{\Gamma(1+\alpha)^2}<0.$$

It follows from the Jury Test that the fixed point is unstable. □

Theorem 1 For the tumor-lymphocyte system (3), if $r>d$ and $\sigma<\frac{d}{r}<1$, the fixed point $\left(\frac{1-\sigma}{r-d}, r\right)$ is unstable.

Proof. Under the condition $r>d$ and $\sigma<\frac{d}{r}<1$, and from (11), we have

$$|p_0|=\left|\frac{h^{\alpha}\left(\frac{\Gamma(1+\alpha)(r\sigma-d)}{r(d-r)}-(\sigma-1)h^{\alpha}\right)}{\Gamma(1+\alpha)^2}+1\right|>1.$$

It follows from the Jury Test that the fixed point is unstable. □

Theorem [21] The zeros of the characteristic polynomial

$$p(\lambda)=\lambda^2+p_1\lambda+p_0,$$

lie inside the unit disk if and only if the following conditions hold:

1. $1+p_1+p_0>0$,
2. $1-p_1+p_0>0$,
3. $1-p_0>0$.

Theorem 2 For the tumor-lymphocyte system (3), if $r>d$ and $\frac{d}{r}<\sigma<1$, the fixed point $\left(\frac{1-\sigma}{r-d}, r\right)$ is asymptotically stable if:

- $$0<\frac{h^{\alpha}}{\Gamma(1+\alpha)}\leq 2r \quad \text{and} \quad \frac{1}{\frac{r}{d-r}-\frac{rh^{\alpha}}{\Gamma(1+\alpha)}}+1<\sigma<1,$$

or

- $$2r<\frac{h^{\alpha}}{\Gamma(1+\alpha)}<2\sqrt{\frac{-dr^2+r^3+r}{r-d}}+2r$$

and

$$\frac{1}{\frac{r}{d-r}-\frac{rh^{\alpha}}{\Gamma(1+\alpha)}}+1<\sigma<\frac{h^{-\alpha}\left(r(r-d)h^{2\alpha}+2d\Gamma(1+\alpha)h^{\alpha}+4r\Gamma(1+\alpha)^2(r-d)\right)}{r(r-d)h^{\alpha}+2r\Gamma(1+\alpha)}.$$

Proof. From (10) and (11), we have: $1+p_1+p_0=-\frac{(\sigma-1)h^{2\alpha}}{\Gamma(1+\alpha)^2}>0$ if $\sigma<1$. Since $\sigma>0$ always holds in our model, we conclude that the condition

$$1+p_1+p_0=-\frac{(\sigma-1)h^{2\alpha}}{\Gamma(1+\alpha)^2}>0$$

is satisfied whenever $0<\sigma<1$. In addition, we have:

$$1-p_1+p_0=\frac{h^{\alpha}\left((\sigma-1)\left(-h^{\alpha}\right)-\frac{2\Gamma(1+\alpha)(d-r\sigma)}{r(d-r)}\right)}{\Gamma(1+\alpha)^2}+4,$$

and

$$1-p_0=\frac{h^{\alpha}\left(\frac{\Gamma(1+\alpha)(d-r\sigma)}{r(d-r)}+(\sigma-1)h^{\alpha}\right)}{\Gamma(1+\alpha)^2}.$$

From the conditions $1+p_1+p_0>0$, $1-p_1+p_0>0$ and $1-p_0>0$, we obtain that for $r>d>0$ and $\frac{d}{r}<\sigma<1$, the fixed point $\left(\frac{1-\sigma}{r-d},r\right)$ is asymptotically stable either if

$$\begin{cases} 0<\dfrac{h^{\alpha}}{\Gamma(1+\alpha)}\leq 2r, \\ \dfrac{1}{\frac{r}{d-r}-\frac{rh^{\alpha}}{\Gamma(1+\alpha)}}+1<\sigma<1, \end{cases}$$

or

$$\begin{cases} 2r<\dfrac{h^{\alpha}}{\Gamma(1+\alpha)}<2\sqrt{\dfrac{-dr^2+r^3+r}{r-d}}+2r, \\ \dfrac{1}{\frac{r}{d-r}-\frac{rh^{\alpha}}{\Gamma(1+\alpha)}}+1<\sigma<\dfrac{h^{-\alpha}\left(r(r-d)h^{2\alpha}+2d\Gamma(1+\alpha)h^{\alpha}+4r\Gamma(1+\alpha)^2(r-d)\right)}{r(r-d)h^{\alpha}+2r\Gamma(1+\alpha)}, \end{cases}$$

where the two ranges of $\frac{h^\alpha}{\Gamma(1+\alpha)}$ correspond to small discretization steps for the first condition, and large discretization steps for the second condition. □

4. Bifurcation analysis

This section investigates the Neimark-Sacker bifurcation of the positive fixed point $(N^*, I^*) = \left(\frac{1-\sigma}{r-d}, r\right)$. For the bifurcation analysis, σ is chosen to be the bifurcation parameter. Biologically, σ corresponds to the lymphocyte influx, meaning that small changes in its value can affect the immune response. Therefore, bifurcation analysis shows how changes in σ can shift the system between different tumor states. Silva et al. [1] showed that changing the value of σ affects both the stability of the system and the position of the fixed point, which makes our choice meaningful. The Neimark-Sacker bifurcation will be studied through center manifold and bifurcation theories [19, 24–27].

Theorem 3 (Neimark-Sacker Bifurcation)

System (3) exhibits a Neimark-Sacker bifurcation at the fixed point $(N^*, I^*) = \left(\frac{1-\sigma}{r-d}, r\right)$, provided the following conditions hold:

1. $r > d > 0$,
2. $0 < \frac{h^\alpha}{\Gamma(1+\alpha)} \leq 2r$,
3. $h^\alpha \neq \frac{\Gamma(1+\alpha)}{d-r}$.

The corresponding critical value of the parameter σ is given by $\sigma^* = \frac{1}{\frac{r}{d-r} - \frac{rh^\alpha}{\Gamma(1+\alpha)}} + 1$, and an attracting invariant closed curve bifurcates from the fixed point E_1 for $\sigma < \sigma^*$.

Proof. The characteristic equation associated with the linearized system (3) at the fixed point $(N^*(\sigma), I^*(\sigma))$ is given by

$$\lambda^2 + p(\sigma)\lambda + q(\sigma) = 0. \tag{12}$$

The eigenvalues corresponding to the characteristic equation (12) can be expressed as

$$\lambda_{1,2} = \frac{-p(\sigma) \pm \sqrt{p(\sigma)^2 - 4q(\sigma)}}{2},$$

where

$$p(\sigma) = \frac{h^\alpha(d - r\sigma)}{r\Gamma(1+\alpha)(d-r)} - 2,$$

and

$$q(\sigma) = \frac{h^\alpha\left(\frac{\Gamma(1+\alpha)(r\sigma - d)}{r(d-r)} - (\sigma-1)h^\alpha\right)}{\Gamma(1+\alpha)^2} + 1.$$

Let

$$\sigma^* = \frac{1}{\frac{r}{d-r} - \frac{rh^\alpha}{\Gamma(1+\alpha)}} + 1, \tag{13}$$

for $0 < \frac{h^\alpha}{\Gamma(1+\alpha)} \leq 2r$, and $r > d > 0$ (see Appendix A.3 for explaining the choice of σ^*). Then,

$$\begin{aligned} q(\sigma^*) =& \frac{h^\alpha \left(\frac{\Gamma(1+\alpha)\left(r\left(\frac{1}{\frac{r}{d-r} - \frac{rh^\alpha}{\Gamma(1+\alpha)}} + 1 \right) - d \right)}{r(d-r)} - \frac{h^\alpha}{\frac{r}{d-r} - \frac{rh^\alpha}{\Gamma(1+\alpha)}} \right)}{\Gamma(1+\alpha)^2} + 1 \\ =& 1, \end{aligned}$$

and

$$\begin{aligned} \lambda_{1,2}(\sigma^*) =& \frac{dh^{2\alpha} - 2dr\Gamma(1+\alpha)h^\alpha - rh^{2\alpha} + 2r^2\Gamma(1+\alpha)h^\alpha + 2r\Gamma(1+\alpha)^2}{2r\Gamma(1+\alpha)\left(\Gamma(1+\alpha) - dh^\alpha + rh^\alpha\right)} \\ & \pm i\frac{h^\alpha\sqrt{r-d}\sqrt{dh^{2\alpha} - 4dr\Gamma(1+\alpha)h^\alpha - rh^{2\alpha} + 4r^2\Gamma(1+\alpha)h^\alpha + 4r\Gamma(1+\alpha)^2}}{2r\Gamma(1+\alpha)\left(\Gamma(1+\alpha) - dh^\alpha + rh^\alpha\right)} \\ =& a \pm ib. \end{aligned}$$

Under condition (13), we have $|\lambda_{1,2}(\sigma)| = (q(\sigma))^{\frac{1}{2}}$ and

$$\sigma_1 = \left.\frac{d|\lambda_{1,2}(\sigma)|}{d\sigma}\right|_{\sigma=\sigma^*} = \frac{h^\alpha\left(\frac{\Gamma(1+\alpha)}{d-r} - h^\alpha\right)}{2\Gamma(1+\alpha)^2} \neq 0.$$

Since $\sigma_1 \neq 0,$ it follows that

$$h^\alpha \neq \frac{\Gamma(1+\alpha)}{d-r}.$$

In addition,

$$p(\sigma^*) \neq 0,\ 1 \text{ that is } p(\sigma^*) = \frac{-2r + h(h-2r)(-d+r)}{r(1-dh+hr)} \neq 0,\ 1.$$

This leads to

$$0 < \frac{h^\alpha}{\Gamma(1+\alpha)} \leq 2r, \text{ and } 0 < d < r.$$

Then we obtain that $\lambda_{1,2}^n(\sigma^*) \neq 0$ for $n = 1, 2, 3, 4$ (non resonance condition).
Letting $u = N - \dfrac{1-\sigma}{r-d}$ and $v = I - r$. Therefore, the map (3) becomes

$$\begin{pmatrix} u \\ v \end{pmatrix} \to \begin{pmatrix} u - \dfrac{(\sigma-1)vh^\alpha}{\Gamma(1+\alpha)(d-r)} - \dfrac{uvh^\alpha}{\Gamma(1+\alpha)} \\ \\ -\dfrac{u(d-r)h^\alpha}{\Gamma(1+\alpha)} + \dfrac{vh^\alpha(r\sigma-d)}{r\Gamma(1+\alpha)(d-r)} + v + \dfrac{uvh^\alpha}{\Gamma(1+\alpha)} \end{pmatrix}. \tag{14}$$

Now substitute σ^* in (14), we obtain

$$\begin{pmatrix} u \\ v \end{pmatrix} \to \begin{pmatrix} 1 & -\dfrac{h^\alpha}{r(\Gamma(1+\alpha)+(r-d)h^\alpha)} \\ \\ -\dfrac{(d-r)h^\alpha}{\Gamma(1+\alpha)} & \dfrac{(d-r)h^{2\alpha}}{r\Gamma(1+\alpha)(r-d)h^\alpha + r\Gamma(1+\alpha)^2} + 1 \end{pmatrix} \begin{pmatrix} u \\ v \end{pmatrix} + \begin{pmatrix} -\dfrac{uvh^\alpha}{\Gamma(1+\alpha)} \\ \\ \dfrac{uvh^\alpha}{\Gamma(1+\alpha)} \end{pmatrix}. \tag{15}$$

Let

$$T = \begin{pmatrix} -\dfrac{\sqrt{(r-d)\begin{pmatrix} dh^{2\alpha} - 4dr\Gamma(\alpha+1)h^\alpha - rh^{2\alpha} \\ +4r^2\Gamma(\alpha+1)h^\alpha + 4r\Gamma(\alpha+1)^2 \end{pmatrix}}}{2r(d-r)\left(-\Gamma(\alpha+1) + dh^\alpha - rh^\alpha\right)} & \dfrac{rh^\alpha - dh^\alpha}{2r(d-r)\left(-\Gamma(\alpha+1) + dh^\alpha - rh^\alpha\right)} \\ \\ 0 & 1 \end{pmatrix}$$

(see Appendix A.4 for the choice of T).

By applying the translation $\begin{pmatrix} u \\ v \end{pmatrix} = T \begin{pmatrix} X \\ Y \end{pmatrix}$, map (15) takes the form

$$\begin{pmatrix} X \\ Y \end{pmatrix} \to \begin{pmatrix} a & -b \\ \\ b & a \end{pmatrix} \begin{pmatrix} X \\ Y \end{pmatrix} + \begin{pmatrix} F_1(X,Y) \\ \\ F_2(X,Y) \end{pmatrix}, \tag{16}$$

where

$$F_1(X,Y) = -\frac{X\,Y\,h^\alpha\left(\left(-2dr+2r^2+1\right)h^\alpha + 2r\Gamma(1+\alpha)\right)}{2r\Gamma(1+\alpha)\left(\Gamma(1+\alpha)+(r-d)h^\alpha\right)}$$

$$- \frac{Y^2\, h^{\alpha}\,(dh^{\alpha} - rh^{\alpha})\left(\left(-2dr + 2r^2 + 1\right)h^{\alpha} + 2r\Gamma(1+\alpha)\right)}{2r\Gamma(1+\alpha)\,(\Gamma(1+\alpha) + (r-d)h^{\alpha})\,\sqrt{(d-r)\,((r-d)h^{2\alpha} + 4r\Gamma(1+\alpha)(d-r)h^{\alpha} - 4r\Gamma(1+\alpha)^2)}},$$

$$F_2(X,Y) = -\frac{h^{\alpha}\,(dh^{\alpha} - rh^{\alpha})}{2r\Gamma(1+\alpha)(d-r)\,((d-r)h^{\alpha} - \Gamma(1+\alpha))}Y^2$$

$$- \frac{h^{\alpha}\sqrt{(d-r)\,((r-d)h^{2\alpha} + 4r\Gamma(1+\alpha)(d-r)h^{\alpha} - 4r\Gamma(1+\alpha)^2)}}{2r\Gamma(1+\alpha)(d-r)\,((d-r)h^{\alpha} - \Gamma(1+\alpha))}X\,Y,$$

(See Appendix A.5 for the computational details of equation (16)).

Observe that (16) follows the structure of the center manifold, where the coefficient k is provided in [24] as

$$k = -\mathrm{Re}\left[\frac{(1-2\lambda)\bar{\lambda}^2}{1-\lambda}\xi_{11}\xi_{20}\right] - \frac{1}{2}|\xi_{11}|^2 - |\xi_{02}|^2 + \mathrm{Re}(\bar{\lambda}\xi_{21}),$$

where

$$\xi_{20} = \frac{1}{8}\left[(F_{1XX} - F_{1YY} + 2F_{2XY}) + i(F_{2XX} - F_{2YY} - 2F_{1XY})\right],$$

$$\xi_{11} = \frac{1}{4}\left[(F_{1XX} + F_{1YY}) + i(F_{2XX} + F_{2YY})\right],$$

$$\xi_{02} = \frac{1}{8}\left[(F_{1XX} - F_{1YY} - 2F_{2XY}) + i(F_{2XX} - F_{2YY} + 2F_{1XY})\right],$$

$$\xi_{21} = \frac{1}{16}\left[(F_{1XXX} + F_{1XYY} + F_{2XXY} + F_{2YYY}) + i(F_{2XXX} + F_{2XYY} - F_{1XXY} - F_{1YYY})\right].$$

Thus, a calculation gives

$$k = \frac{n_1}{8r^3\Gamma(1+\alpha)^3\,(\Gamma(1+\alpha) + (r-d)h^{\alpha})^3} < 0,$$

where

$$n_1 = h^{2\alpha}\Big[(d-r)(-dr + r^2 + 1)^2 h^{4\alpha} + r\Gamma(1+\alpha)\Big((d-r)(r(d-r) - 2)(r(d-r) - 1)h^{3\alpha}$$

$$+ r\Gamma(1+\alpha)\big(-3(r-d)(-dr + r^2 + 1)h^{2\alpha} + \Gamma(1+\alpha)(3r(d-r) - 1)h^{\alpha} - r\Gamma(1+\alpha)^2\big)\Big)\Big],$$

for $0 < \dfrac{h^{\alpha}}{\Gamma(1+\alpha)} \leq 2r$, $r > d > 0$, and $h^{\alpha} < \dfrac{\Gamma(1+\alpha)}{d-r}$ or $h^{\alpha} > \dfrac{\Gamma(1+\alpha)}{d-r}$. □

See Appendix A.6 for the computational details of the coefficient k.

5. Chaos control

From a biological standpoint, chaotic behavior near a fixed point in discrete-time systems caused by Neimark-Sacker bifurcation is not preferred, as it may cause highly unpredictable tumor growth and unstable tumor-immune interactions. To control this chaotic behavior, we apply chaos control techniques to the system by introducing small perturbations, which help stabilize unstable trajectories and restore order to the dynamics. To suppress the chaotic behavior at the unstable fixed point of system (3) and ensure its stabilization, the feedback control method [12, 25, 28, 29] was employed. The controlled system corresponding to system (3) is given by

$$\begin{cases} N_{n+1} = N_n + \dfrac{h^\alpha}{\Gamma(1+\alpha)}\left(rN_n - N_nI_n\right) + u_n \\ \\ I_{n+1} = I_n + \dfrac{h^\alpha}{\Gamma(1+\alpha)}\left(\sigma - \dfrac{1}{r}I_n - dN_n + N_nI_n\right) \end{cases} \tag{17}$$

where $u_n = -k_1(N_n - N^*) - k_2(I_n - I^*)$ is feedback controlling force at the positive fixed point E_1. It is observed in [30] that treatment success can be improved if immunotherapy is taken into account in the presence of chemotherapy. While chemotherapy primarily focuses on attacking the tumor, immune-based therapies, such as Interleukin-2 (IL-2), help the body's immune system work better. IL-2 is a cytokine that boosts immune function and helps certain immune cells ($CD8^+$ T cells) grow and attack tumors. In treatment, IL-2 is often administered in combination with chemotherapy and in conjunction with Tumor-Infiltrating Lymphocyte (TIL) therapy, where highly activated $CD8^+$ T cells are injected into the body to strengthen the immune response. This idea fits well with the way we describe the feedback gains in our model from a biological perspective, k_1 represents how strongly we suppress tumor growth using chemotherapy, while k_2 represents the enhancement of the immune response through treatment such as IL-2 or TIL, which helps immune cells attack the tumor [31, 32]. Moreover, the control gains k_1 and k_2 must remain within realistic biological ranges. Large values may correspond to toxic side effects [30], whereas low values would lead to therapeutically ineffective responses. Changing these parameters in our model simulates the effects of combined therapies, showing how feedback-controlled strategies can stabilize tumor dynamics and prevent chaotic behavior that may cause relapse or uncontrolled growth. This approach matches emerging clinical strategies that adjust treatment dosing and timing to maintain tumor dormancy and improve patient outcomes [33, 34]. Our results highlight the importance of including feedback mechanisms in treatment design to reduce unpredictable tumor responses and optimize therapy effectiveness.

The Jacobian matrix evaluated at the fixed point $E_1 = \left(\dfrac{1-\sigma}{r-d}, r\right)$ for the controlled system (17) is expressed as

$$J_k\left(\frac{1-\sigma}{r-d}, r\right) = \begin{pmatrix} 1-k_1 & -\dfrac{(1-\sigma)h^\alpha}{\Gamma(1+\alpha)(r-d)} - k_2 \\ \\ \dfrac{(r-d)h^\alpha}{\Gamma(1+\alpha)} & \dfrac{h^\alpha\left(\frac{1-\sigma}{r-d} - \frac{1}{r}\right)}{\Gamma(1+\alpha)} + 1 \end{pmatrix}.$$

The characteristic equation of the Jacobian matrix $J_k\left(\dfrac{1-\sigma}{r-d}, r\right)$ is

$$\lambda^2 + p_3\lambda + p_2 = 0, \tag{18}$$

where

$$p_3 = \left(\frac{h^\alpha(d-r\sigma)}{r\Gamma(1+\alpha)(d-r)} + k_1 - 2\right),$$

and

$$p_2 = \frac{h^\alpha\left((\sigma-1)(-h^\alpha) - \frac{\Gamma(1+\alpha)\left(d^2k_2r - d\left(k_1+2k_2r^2-1\right)+(k_1-1)r\sigma+k_2r^3\right)}{r(d-r)}\right)}{\Gamma(1+\alpha)^2} - k_1 + 1.$$

Assume that λ_1 and λ_2 are the eigenvalues of (18), then

$$\lambda_1 + \lambda_2 = \frac{h^\alpha(r\sigma-d)}{r\Gamma(1+\alpha)(d-r)} - k_1 + 2, \tag{19}$$

and

$$\lambda_1\lambda_2 = \frac{h^\alpha\left((\sigma-1)(-h^\alpha) - \frac{\Gamma(1+\alpha)\left(d^2k_2r - d\left(k_1+2k_2r^2-1\right)+(k_1-1)r\sigma+k_2r^3\right)}{r(d-r)}\right)}{\Gamma(1+\alpha)^2} - k_1 + 1. \tag{20}$$

To find the lines of marginal stability, we must solve the equations $\lambda_1 = \pm 1$ and $\lambda_1\lambda_2 = 1$. These conditions confirm that the eigenvalues λ_1 and λ_2 have absolute value less than 1.

Assuming that $\lambda_1\lambda_2 = 1$, it follows from (20) that

$$L_1\colon k_2\left(\frac{(r-d)h^\alpha}{\Gamma(1+\alpha)}\right) + k_1\left(\frac{h^\alpha(d-r\sigma)}{r\Gamma(1+\alpha)(d-r)} - 1\right) = -\frac{h^\alpha\left(\frac{\Gamma(1+\alpha)(r\sigma-d)}{r(d-r)} - (\sigma-1)h^\alpha\right)}{\Gamma(1+\alpha)^2}.$$

Assuming that $\lambda_1 = 1$, and using equations (19) and (20), we obtain

$$L_2\colon k_2\left(\frac{(d-r)h^\alpha}{\Gamma(1+\alpha)}\right) + k_1\left(\frac{h^\alpha(r\sigma-d)}{r\Gamma(1+\alpha)(d-r)}\right) = -\frac{(\sigma-1)h^{2\alpha}}{\Gamma(1+\alpha)^2}.$$

Assuming that $\lambda_1 = -1$, and using equations (19) and (20), we obtain

$$L_3\colon k_2\left(\frac{(r-d)h^{\alpha}}{\Gamma(1+\alpha)}\right)+k_1\left(\frac{h^{\alpha}(d-r\sigma)}{r\Gamma(1+\alpha)(d-r)}-2\right)=-\left(\frac{h^{\alpha}\left((\sigma-1)\left(-h^{\alpha}\right)-\frac{2\Gamma(1+\alpha)(d-r\sigma)}{r(d-r)}\right)}{\Gamma(1+\alpha)^2}+4\right).$$

Within the triangular region bounded by the straight lines L_1, L_2, and L_3, the eigenvalues remain stable.

6. Numerical simulations

In this section, we will confirm the above theoretical results by numerical simulations, including time series plots, phase portraits, a bifurcation diagram, Lyapunov exponents, and an analysis of the effect of the fractional order α on the dynamics of the system (3). Since system (3) is nondimensional, n is considered as the discrete time step in all simulations.

Table 1. Nondimensional parameter values used in the simulations [2, 35]

Parameter	Interpretation	Numerical value	Baseline value	Figures
r	Proliferation rate of tumor cells	0.1, 1, 2	2	All except Figure 1
d	Lymphocyte death from tumor cell growth	0.05, 0.2	0.2	All except Figure 1
σ	Lymphocyte influx	0.5, 1, 3	Varied	

Starting with the first fixed point $E_0 = (0,\ r\sigma)$, we verify the theoretical results given in Lemma 1 using time series plots. The parameter values listed in Table 1 were chosen based on previous tumor-immune model studies [2, 35]. Figure 1(a) shows that the solution, starting from the initial value $(0.5,\ 2.5)$, stays close to the fixed point $(0,\ 3)$ and eventually converges to it. This matched the expected behavior from Lemma 1(i), which confirms that the fixed point is asymptotically stable. Figure 1(b) illustrates the behavior described in Lemma 1(ii), with the initial value $(0.02,\ 0)$, the lymphocyte population $(I(n)$, black sketch) stays close to the fixed point $(0,\ 0.05)$, while the tumor cell population $(N(n)$, red sketch) increases over time. This confirms that the fixed point is a saddle point. Figure 1(c) shows that the solution with the initial value $(0.02,\ 2.01)$ remains close to the fixed point $(0,\ 2)$ but does not fully converge to it. This behavior is consistent with Lemma 1(iii): when $r = d$, the fixed point is stable but not asymptotically stable. In Figure 1(d), the fixed point is semi-stable from the right. The initial value $(0.02,\ 2.01)$, which lies above the fixed point $(0,\ 2)$, leads to a solution that remains close to the fixed point over time but does not converge to it. This behavior is consistent with the sign of $\hat{f}''(0) = -2.34112 < 0$, confirming semi-stability from the right, as stated in Lemma 1(iii) for the case $r \neq d$.

For Lemma 1(ii), to show how the stability changes from a stable fixed point to a saddle point as σ crosses the upper bound, we give a short numerical example. For $h = 0.05,$ and $\alpha = 0.95$, we find that $r > 0.0296359$ which implies that $|\lambda_2| < 1$. Choose $r = 0.1$, the stability condition becomes $1 < \sigma < 338.4284$, and

- If $\sigma = 300$, then $|\lambda_1| = 0.772228 < 1$. (stable)
- If $\sigma = 338.4284$, then $|\lambda_1| = 1$. (boundary case)
- If $\sigma = 340$, then $|\lambda_1| = 1.00931 > 1$. (saddle, unstable)

This confirms the result of Lemma 1, where if $1 < \sigma < 1 + \frac{2\Gamma(1+\alpha)}{rh^{\alpha}}$, the fixed point is asymptotically stable, and if $\sigma > 1 + \frac{2\Gamma(1+\alpha)}{rh^{\alpha}}$, the fixed point is a saddle.

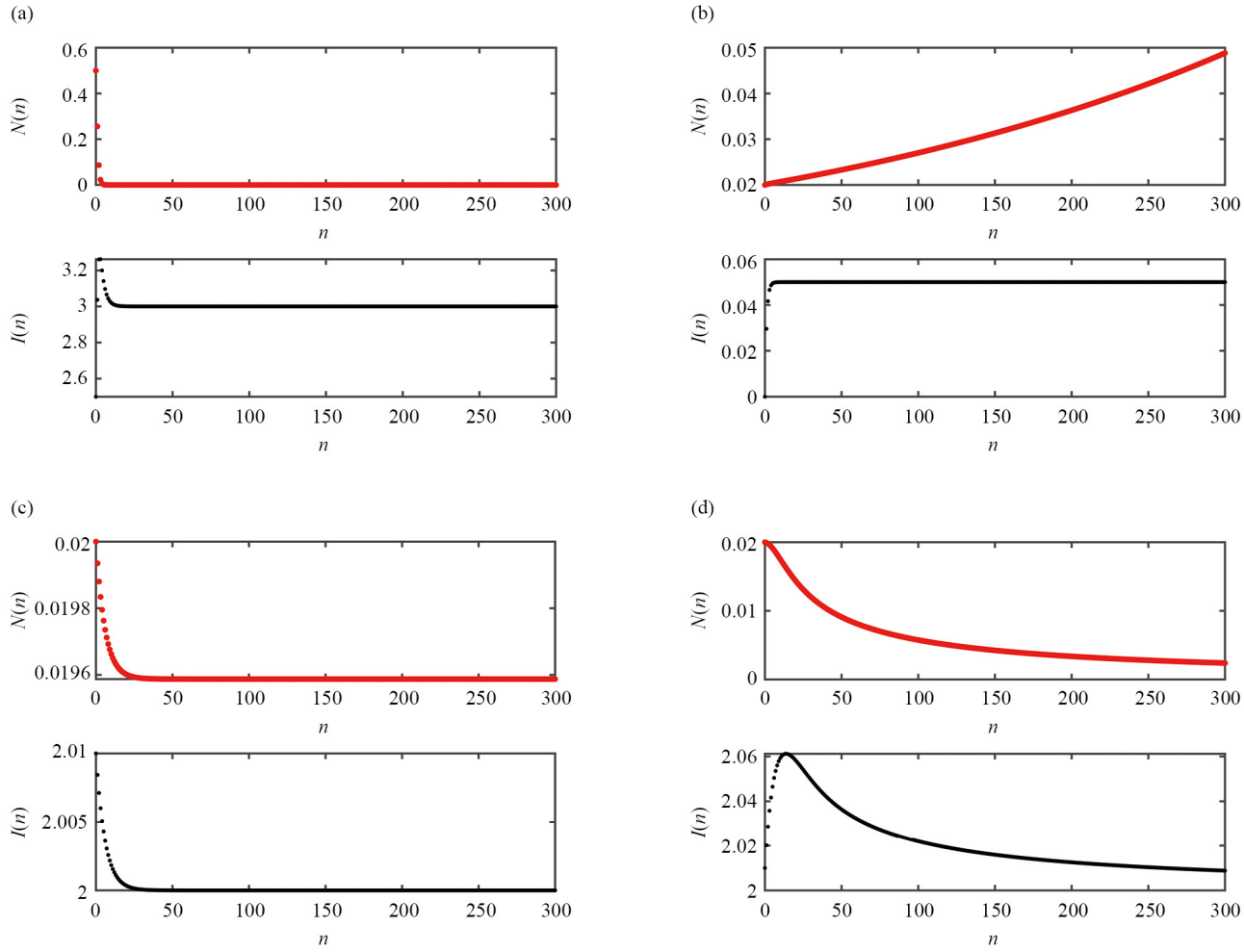

Figure 1. Time series plots of tumor cell population $N(n)$ and lymphocyte population $I(n)$ for the fixed point $(0,\ r\sigma)$: (a) $h = 0.3$, $\alpha = 0.95$, $r = 1$, $d = 0.2$, $\sigma = 3$, $N(0) = 0.5$, $I(0) = 2.5$; (b) $h = 0.05$, $\alpha = 0.95$, $r = 0.1$, $d = 0.05$, $\sigma = 0.5$, $N(0) = 0.02$, $I(0) = 0$; (c) $h = 0.3$, $\alpha = 0.95$, $r = d = 2$, $\sigma = 1$, $N(0) = 0.02$, $I(0) = 2.01$; and (d) $h = 0.3$, $\alpha = 0.95$, $r = 2$, $d = 0.2$, $\sigma = 1$, $N(0) = 0.02$, $I(0) = 2.01$

Next, we verify the theoretical results for the second fixed point $E_1 = \left(\dfrac{1-\sigma}{r-d},\ r\right)$. Again, with our set of parameter values taken from Table 1. The stability region of the positive fixed point can be obtained from Theorem 2 as $0.432277 < \sigma < 1$. It is seen from the Figures 2(a) and 2(b) show that the positive fixed point of the system is locally asymptotically stable. For $\sigma = 0.8$, the system exhibits almost no oscillatory behavior. In contrast, when σ is reduced to 0.5, tumor cells display damped oscillatory behavior that eventually reaches a steady state. In both cases, this phase is biologically referred to as the tumor's dormant state. Moreover, Figures 2(a) and 2(b) show that the tumor cell population stabilizes at the fixed points $(0.277778,\ 2)$ and $(0.111111,\ 2)$, respectively. The system becomes stable and reaches these fixed points after approximately 100 and 300 discrete time steps, respectively. We can observe that increasing σ speeds up the stabilization of the tumor cell population. The threshold value for stability is the decrease of the lymphocyte flow constant to the critical value $\sigma^* = 0.432277$. This value also represents the threshold for the dormancy phase of tumor cells, where tumor cells exhibit quasi-periodic behavior with maintained oscillations, as shown in Figure 2(c). For $\sigma = 0.4$, Figure 2(d) shows that the tumor cell population fails to stabilize at the fixed point $(0.333333,\ 2)$, where tumor cells display uncontrolled growth with higher amplitude oscillations.

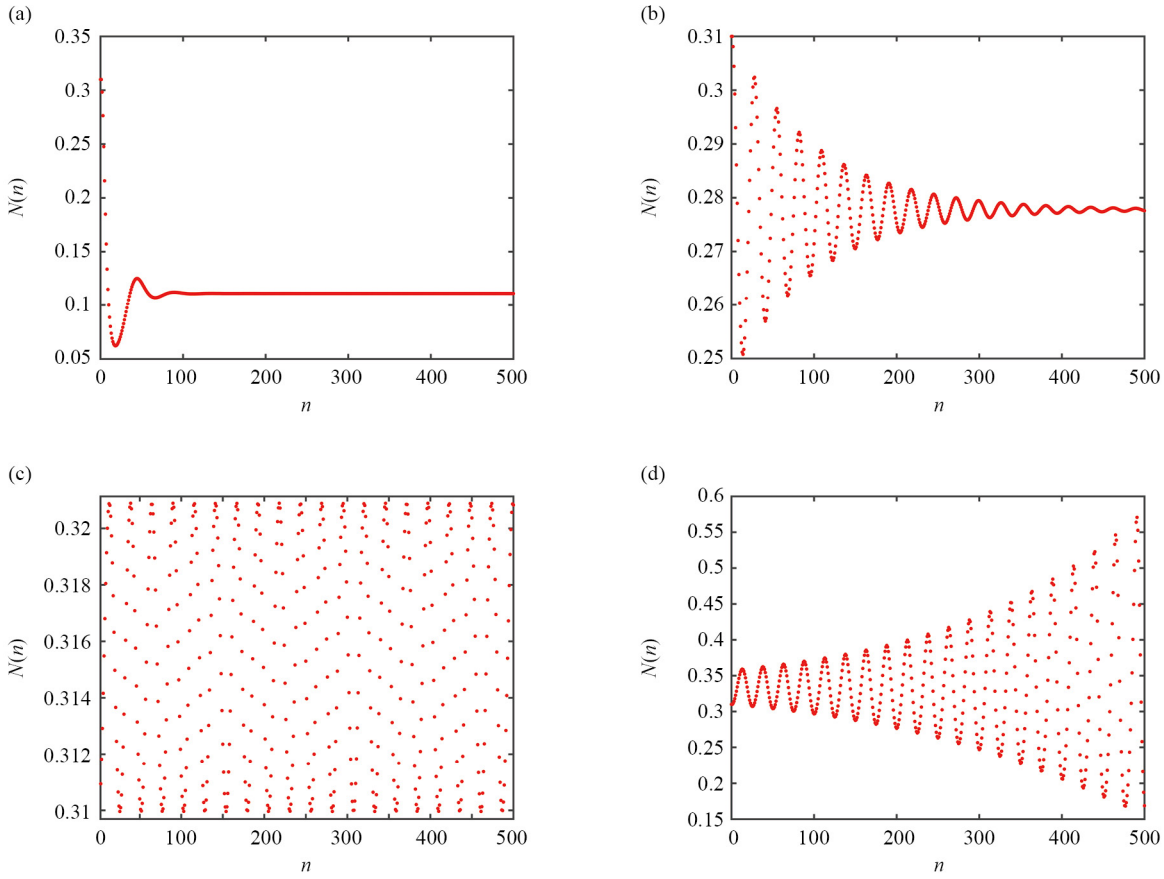

Figure 2. Time series plots of the tumor cell population $N(n)$ under varying the parameter σ, with fixed parameters $r = 2$, $d = 0.2$, $h = 0.3$, $\alpha = 0.95$, $N(0) = 0.31$, and $I(0) = 2$: (a) $\sigma = 0.8$; (b) $\sigma = 0.5$; (c) $\sigma = 0.432277$ and (d) $\sigma = 0.4$

For the simulation of the bifurcation analysis in Section 4, we use parameter values in Figure 2 at the bifurcation point $\sigma^* = 0.432277$. The Jacobian matrix of system (3) at the fixed point $(0.315402, 2)$ is given by

$$J(0.315402, 2) = \begin{pmatrix} 1 & -0.102555 \\ 0.585281 & 0.939977 \end{pmatrix},$$

and its eigenvalues are $0.969988 \pm 0.243152i$.

Now, $|\lambda_{1,2}(\sigma)| = |0.969988 \pm 0.243152i| = 1$. Furthermore, it is easy to see that $\left.\frac{d|\lambda_{1,2}(\sigma)|}{d\sigma}\right|_{\sigma=\sigma^*} = -0.143184 \neq 0$. In addition, $p(\sigma^*) = -1.93998 \neq 0,\ 1,$ which leads to $\lambda^n_{1,2}(\sigma^*) \neq 0$ for $n = 1, 2, 3, 4$ (non resonance condition). Furthermore,

$$\lambda_{1,2}(\sigma) = 0.969988 \pm 0.243152i \neq 1,$$

$$\lambda^2_{1,2}(\sigma) = 0.881754 \pm 0.471709i \neq 1,$$

$$\lambda_{1,2}^{3}(\sigma) = 0.740594 \pm 0.671952i \neq 1,$$

$$\lambda_{1,2}^{4}(\sigma) = 0.55498 \pm 0.831863i \neq 1,$$

which confirms the non-resonance condition. From the above results, all conditions for the existence of Neimark-Sacker bifurcation at the positive fixed point are verified.

From center manifold theory, we apply the translation $\begin{pmatrix} u \\ v \end{pmatrix} = T \begin{pmatrix} X \\ Y \end{pmatrix}$. It follows that map (16) takes the form

$$\begin{pmatrix} X \\ Y \end{pmatrix} \to \begin{pmatrix} 0.969988 & 0.243151 \\ -0.243151 & 0.969988 \end{pmatrix} \begin{pmatrix} X \\ Y \end{pmatrix} + \begin{pmatrix} 0.0421913Y^2 - 0.341829XY \\ -0.135084XY + 0.0166731Y^2 \end{pmatrix},$$

and some complex calculations give $k = -0.0155355 < 0$, thus an attracting invariant closed curve bifurcates from the fixed point for $\sigma < \sigma^* = 0.432277$.

Figure 3 shows the confirmation of Theorem 3 and confirms the occurrence of a Neimark-Sacker bifurcation in Figure 2(c), where the bifurcation occurs at the bifurcation point $\sigma^* = 0.432277$.

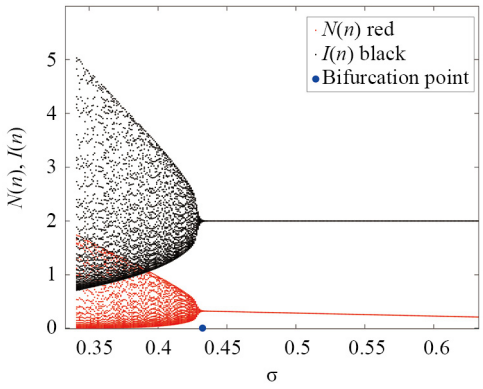

Figure 3. Bifurcation diagram for system (3) in (σ, N) plane and (σ, I) plane for $r = 2$, $d = 0.2$, $h = 0.3$, $\alpha = 0.95$, $N(0) = 0.31$, and $I(0) = 2$, and the bifurcation point $\sigma^* = 0.432277$

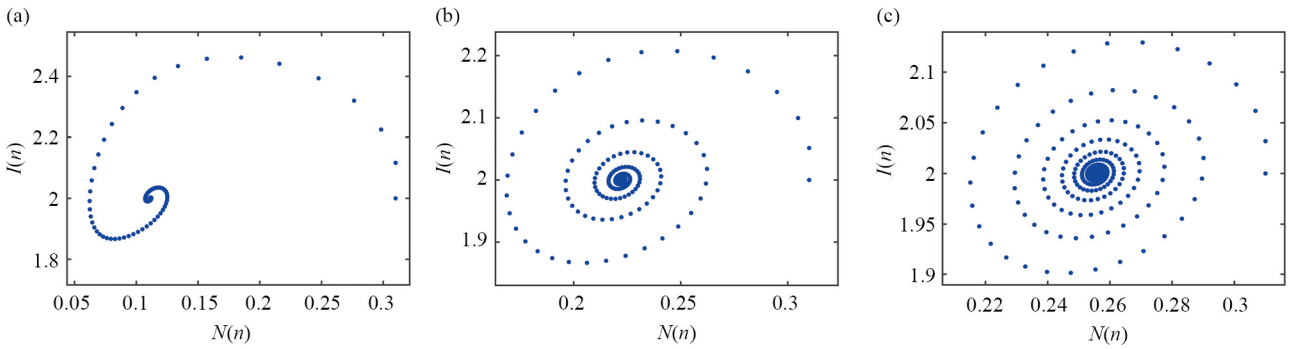

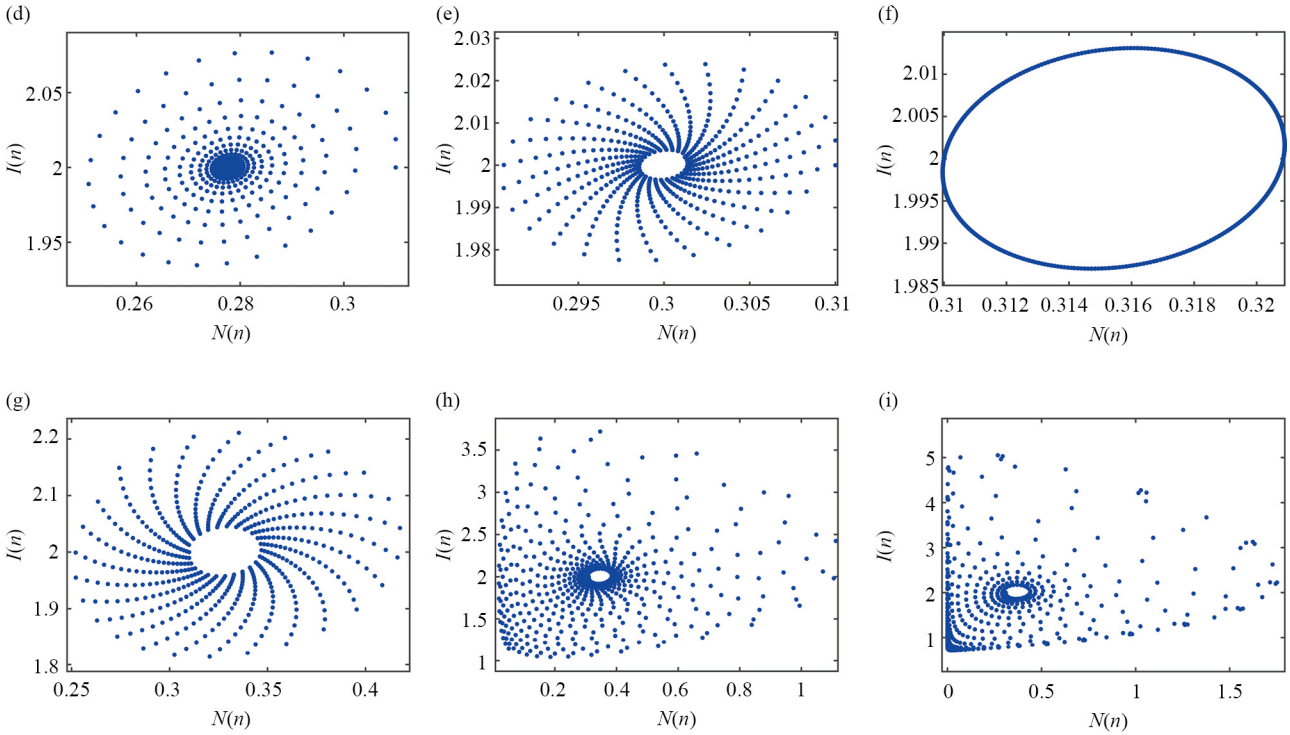

Figure 4. Phase portrait of tumor cell population $N(n)$ and lymphocyte population $I(n)$ under varying the parameter σ, with fixed parameters $r = 2$, $d = 0.2$, $h = 0.3$, $\alpha = 0.95$, $N(0) = 0.31$, and $I(0) = 2$: (a) $\sigma = 0.8$; (b) $\sigma = 0.6$; (c) $\sigma = 0.54$; (d) $\sigma = 0.5$; (e) $\sigma = 0.46$; (f) $\sigma = 0.432277$; (g) $\sigma = 0.41$; (h) $\sigma = 0.38$ and (i) $\sigma = 0.34$

It can also be seen from the phase portrait diagram, Figure 4, that the system exhibits different dynamic behaviors, such as a stable fixed point for (a) $\sigma = 0.8$, (b) $\sigma = 0.6$, (c) $\sigma = 0.54$, (d) $\sigma = 0.5$, (e) $\sigma = 0.46$, and for (f) $\sigma = 0.432277$ there is a limit cycle, and an unstable fixed point for σ less than 0.432277.

In a dynamical system, Lyapunov exponents are a powerful tool for illustrating the behavior of the system, particularly in detecting and measuring chaos. Mathematically, Lyapunov exponents measure the rate at which the nearby trajectories converge or diverge [36]. For the discrete system $x_{n+1} = f(x_n)$, $x_n \in \mathbb{R}^m$, let $J(x_0) = D_x f(x)\big|_{x=x_0}$ be the Jacobian. Following Marco Sandri's algorithm based on QR decomposition [36], write $J(x_0)$ as $J(x_0) = Q_1 R_1$. For $k = 2, 3, \ldots, n$, define $J_k^* = J\big(f^{k-1}(x_0)\big)\, Q_{k-1}$, and decompose it to obtain $J_k^* = Q_k R_k$. By the chain rule, we obtain $D_x f^n(x_0) = Q_n R_n \cdots R_1$, where Q_j is an orthogonal matrix with $Q_j^T Q_j = I$, and R_j is an upper triangular matrix for $j = 1, 2, \ldots n$. Hence, the Lyapunov exponents can be computed as

$$\lambda_i = \lim_{n\to\infty} \frac{1}{n} \ln v_{ii}^{(n)},$$

where $v_{ii}^{(n)}$ is the i-th diagonal element of the product $R_n R_{n-1} \cdots R_1$ for $i = 1, 2 \ldots m$. If at least one Lyapunov exponent is positive, then the system exhibits chaos [37]. Figure 5 illustrates the presence of chaotic regions and periodic orbits in the parametric space, where it is observed that some of the Lyapunov exponents are positive, while others are negative. Hence, stable fixed points or stable period windows exist in the chaotic region. For instance, as seen in Figure 5, chaos is confirmed at $\sigma = 0.38$, where the maximum Lyapunov exponent is calculated to be $0.0057 > 0$. This value was obtained using Marco Sandri's Mathematica package [36], running 1,000 iterations, the first 100 iterations are removed as transients, and the QR decomposition is applied at every iteration.

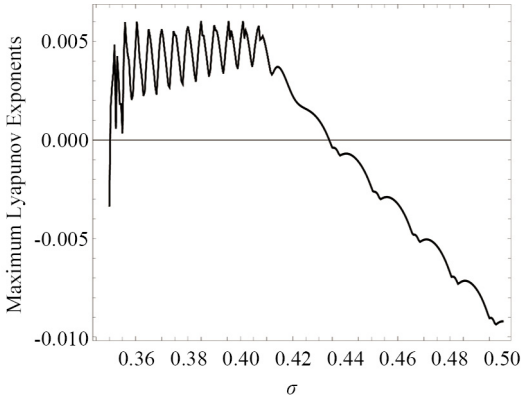

Figure 5. Maximum Lyapunov exponent for system (3) corresponding to Figure 3 for $r = 2$, $d = 0.2$, $h = 0.3$, $\alpha = 0.95$, $N(0) = 0.31$, and $I(0) = 2$. The computation uses 1,000 iterations with the first 100 removed as transients

As shown by the numerical simulations above, the tumor flow parameter σ plays a critical role in the dynamic behavior of the model. Lymphocyte influx σ may decrease due to low production or reduced migration of immune cells (especially $CD8^+$ T cells and Natural Killer (NK) cells) to the tumor site, weakening the immune system's ability to control tumor growth. When the lymphocyte flow parameter is reduced, the balance between the immune system and tumor cells shifts toward the tumor, allowing it to reactivate and proliferate within its local environment. This can accelerate processes such as proliferation, invasion, and angiogenesis. In particular, when σ falls below the critical threshold of 0.432277, the tumor may return in unexpected ways, escape the body's control systems, or develop resistance to therapy, showing chaotic behavior in tumor cells (Figures 2-5).

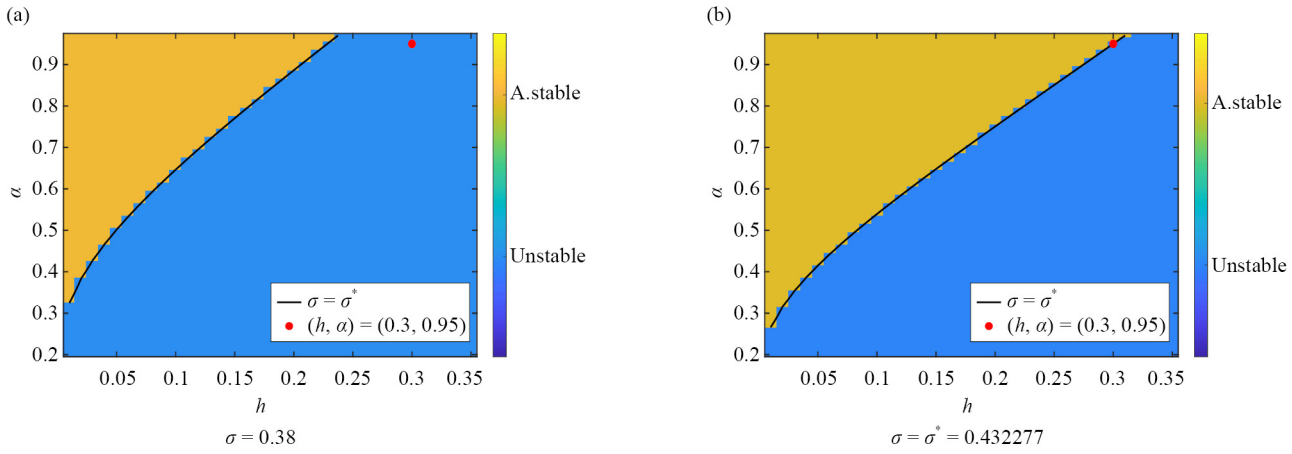

Figure 6. Stability region of E_1 in the (h, α) plane according to Theorem 2 for $r = 2$ and $d = 0.2$

Figure 6 shows the stability region of the fixed point $E_1 = \left(\frac{1-\sigma}{r-d}, r\right)$ for $r > d$, and $\frac{d}{r} < \sigma < 1$ in the (h, α) plane, illustrates the sensitivity of how the stability region varies as h and α vary. The brown region in Figure 6 indicates the stable region of the fixed point E_1. The black curve $\sigma = \sigma^*$ indicates where the fixed point loses stability through a Neimark-Sacker bifurcation. The blue region represents the unstable region. To relate these results to the Lyapunov analysis in Figure 5, the parameter value $\sigma = 0.38$, which lies in the chaotic regime, is indicated by a red dot in Figure 6(a). Similarly, the critical value $\sigma^* = 0.432277$, at which the Neimark-Sacker bifurcation occurs, is marked in Figure 6(b).

The following paragraph presents the calculation of the specific values for the feedback control parameters k_1 and k_2 (the values were chosen from the triangle stability region in Figure 7) and discusses their biological significance. Numerical simulations were employed to investigate the stabilization of an unstable fixed point using a feedback control method, with Figure 7 illustrating the triangular stability region. Figure 8 shows how the system gradually stabilizes around the fixed point $(0.366667,\ 2)$ as the feedback control parameters k_1 and k_2 increase. In Figure 8(a), when no treatment is given $(k_1 = 0, k_2 = 0)$, both the tumor and lymphocyte populations show large oscillations, indicating chaotic behavior. In this case, the tumor cells exhibit very aggressive behavior, and the immune system fails to destroy the tumor or at least reduce it to a dormant state. In such a situation, it is clear that a treatment will be needed to control the aggressive behavior of tumor cells. For reasons we have previously established from a biological perspective, we will present a treatment combination that includes both chemotherapy k_1 and immune system effects k_2. It is important to note that the chemotherapy and immunotherapy treatments described here are administered simultaneously. The chemotherapy treatment approach is initially administered at a dose specified as $k_1 = 0.1503$ in equation (17), and immunotherapy treatment is applied by injection of activated $CD8^+$ T cells at a ratio of $k_2 = 0.004434$ (Figure 8(b)). In Figure 8(b), as treatment increases slightly, the oscillations decrease, and the solution gradually approaches the fixed point. The second situation involves higher chemotherapy doses and $CD8^+$ T cell injection rates, where $k_1 = 0.5391$ and $k_2 = 0.1821$ (Figure 8(c)). In Figure 8(c), with stronger treatment, the oscillations are almost eliminated, and the previously chaotic fluctuations are fully brought under control. While the tumor cell population can be controlled in both cases, the second case, which includes higher chemotherapy doses and $CD8^+$ T cell injection rates, is more advantageous than the first case because the tumor population can be controlled in a shorter time. This suggests that the intensity of the therapy can fully stabilize the fixed point, bringing the interaction between tumor cells and lymphocytes into a stable and controlled state.

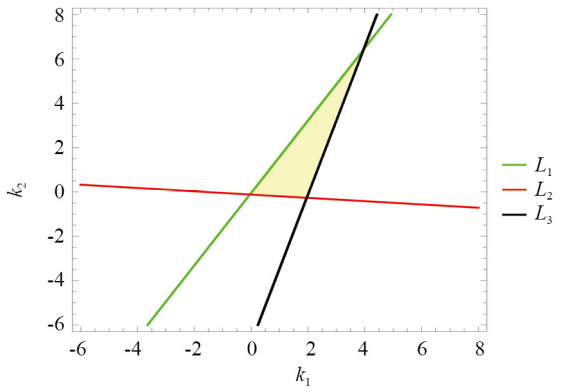

Figure 7. Triangle stability region (shown in yellow) is defined by L_1, L_2, and L_3

Finally, a more detailed investigation of the influence of the fractional order α on the dynamics of system (3) is presented. As it is shown in Figure 9, variations in the value of α lead to noticeably different behaviors in the tumor cell population $N(n)$, highlighting the role of fractional memory in the system behavior over time. Since the fractional operator includes memory, the value of α controls how strongly the system depends on its past states. At $\sigma = 0.5$, decreasing α increases the memory effect, causing the system to exhibit oscillations with both larger amplitudes and extended durations. Such behavior indicates that at low σ, the system becomes more sensitive and complex, and even small changes in α can alter the qualitative nature of the dynamics. In contrast, when $\sigma = 0.8$, the memory effect is largely suppressed, and the trajectories rapidly converge to the fixed point for all values of α. This shows that for higher values of σ, the influence of the fractional-order parameter α becomes weaker, resulting in a more stable dynamical structure that is only weakly affected by variations in α. Overall, these observations confirm that the system is highly sensitive to the fractional order α when σ is low, while at higher values of σ, the dynamics become more stable and less influenced by α.

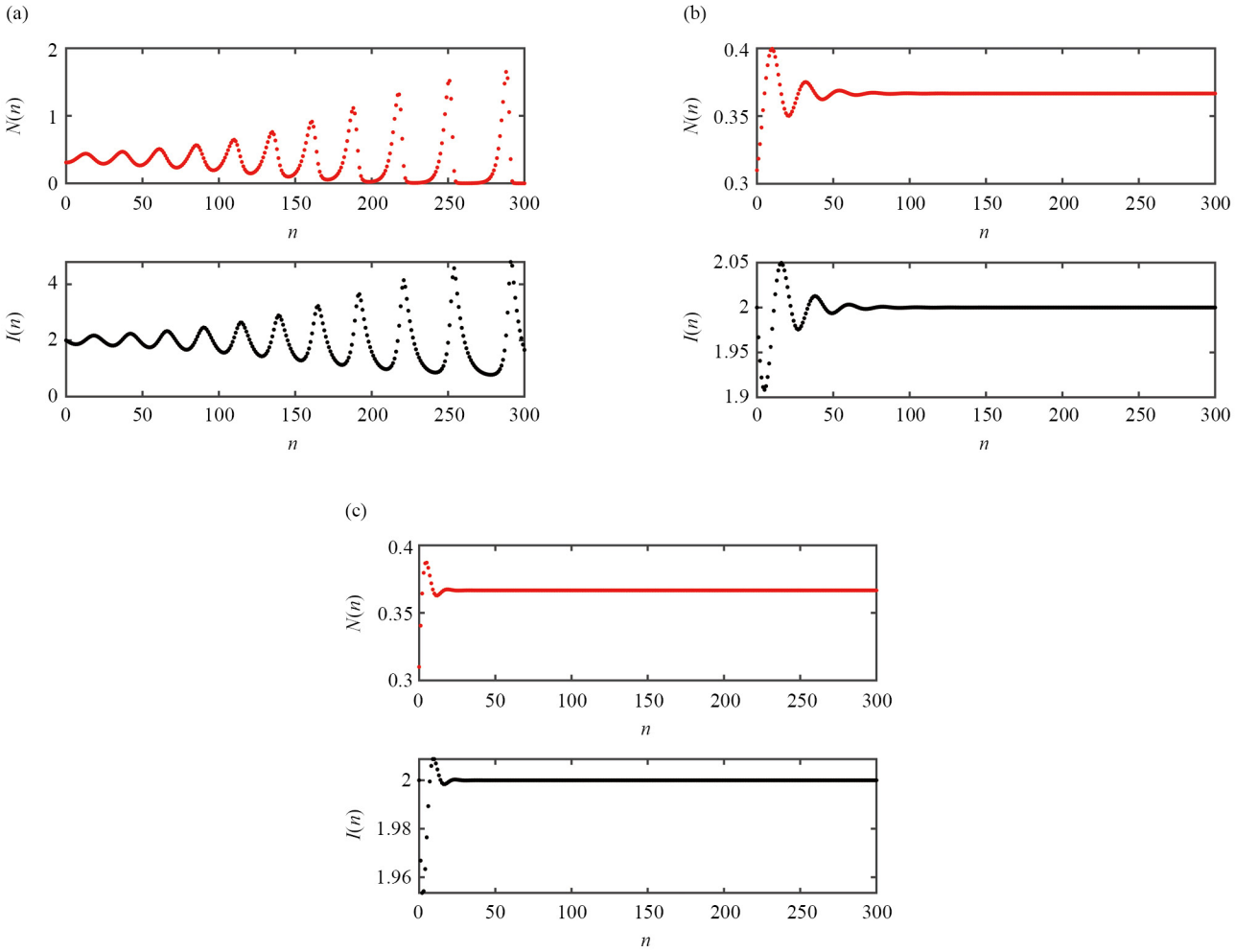

Figure 8. Time series plots of the tumor cell population $N(n)$ and lymphocyte population $I(n)$ for the controlled system (17) for $h = 0.3$, $\alpha = 0.95$, $r = 2$, $d = 0.2$, $\sigma = 0.34$, $N(0) = 0.31$, $I(0) = 2$, under different values of the feedback control parameters k_1 and k_2: (a) $k_1 = 0$ and $k_2 = 0$; (b) $k_1 = 0.1503$ and $k_2 = 0.004434$; (c) $k_1 = 0.5391$ and $k_2 = 0.1821$

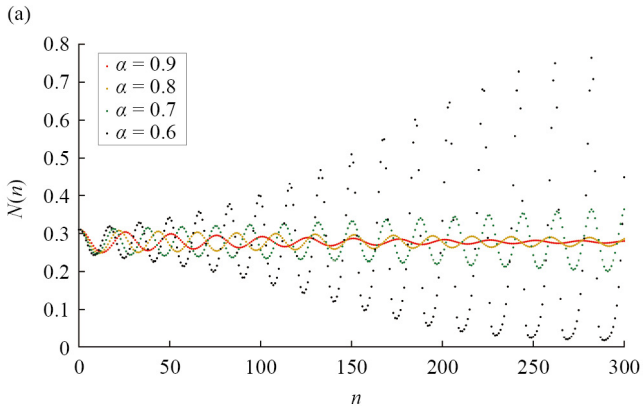

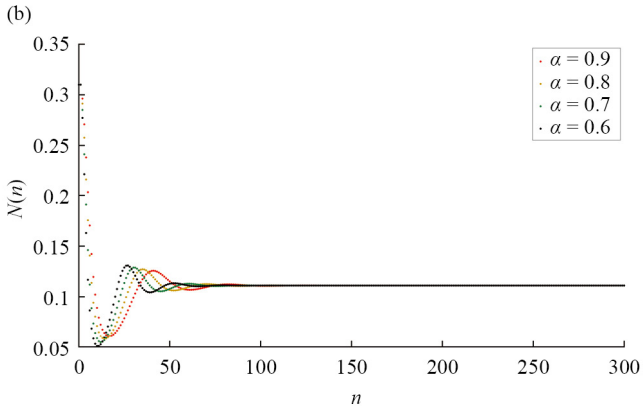

Figure 9. Time series plots of tumor cell population $N(n)$ for different values of α, with fixed parameters $r = 2$, $d = 0.2$, $h = 0.3$, $N(0) = 0.31$, and $I(0) = 2$, (a) $\sigma = 0.5$; (b) $\sigma = 0.8$

7. Conclusions

In this paper, we consider a discrete fractional version of a tumor-immune model, originally proposed by Sotolongo-Costa et al. [2] and extended by Silva et al. [1] to explore cancer dormancy. First, we applied piecewise constant arguments to the fractional order model (1). Then, we analyzed the stability of the two fixed points $E_0 = (0,\ r\sigma)$ and $E_1 = \left(\dfrac{1-\sigma}{r-d},\ r\right)$. For E_0, the stability is analyzed using eigenvalue analysis and the center manifold theory. The stability of the second fixed point, E_1, is analyzed using the Jury test and the Schur-Cohn criterion. For E_1, and for $r < d$ and $\sigma > 1$, our result (Lemma 2) shows that the second fixed point is unstable. This agrees with the result from [2], where the same point was identified as a saddle. For $r > d$ and $0 < \sigma < 1$, our result (Theorems 1 and 2) shows that the second fixed point is stable for $\dfrac{d}{r} < \sigma < 1$ and unstable for $\sigma < \dfrac{d}{r} < 1$. This also agrees with the result from [2]. Additionally, the occurrence of limit cycles in the continuous-time dynamic version of models constructed using both ordinary differential equations [2] and fractional order differential equations [1] is an indication of the presence of a Hopf bifurcation. This result is consistent with the occurrence of a Neimark-Sacker bifurcation at the positive equilibrium point of the discretized model (3). The most significant difference between our model and the models proposed in the aforementioned studies is that our model exhibits chaotic behavior in tumor-immune interactions, which are also observed in experimental data and are more consistent with real-life dynamics. Mathematically, we demonstrated this by showing the existence of positive Lyapunov exponents. Moreover, in section 5, we applied a feedback control method to stabilize chaotic behavior at the unstable fixed point. A combination of chemotherapy and immune-support treatments can be used to reach this goal efficiently. Finally, in section 6, positive Lyapunov exponents are observed, suggesting the presence of chaos in the system. Also, the results show that a smaller σ leads to a system that is highly sensitive to the fractional order α, whereas a higher σ makes the system more stable and less affected by α.

Although our model describes many complex dynamics of tumor-immune interactions, it includes only a few cell types, namely tumor cells and T cells, omitting important components such as macrophages, dendritic cells, and stromal cells. In addition, the absence of spatial structure, stochasticity, and patient heterogeneity should be considered limitations. Future work will address these limitations by extending the model to include additional immune components (e.g., macrophages), introducing stochastic forcing, and fitting the model to experimental tumor-immune time series. Another current area of research is the side effects of cancer treatments and their long-term impacts on patient health, which must also be considered [38, 39]. Our model can be adapted to these newly developed models and, by accounting for treatment side effects, contribute to the formulation of more comprehensive and realistic therapeutic strategies.

Author contributions

All authors read and approved the final manuscript.

Data availability

Code for the main computations and for producing the figures is provided as a supplementary material file and can be found at https://ojs.wiserpub.com/index.php/CM/article/view/8851.

Conflict of interest

The authors declare no competing financial interest.

References

[1] Silva JG, Ribeiro ACO, Camargo RF, Mancera PFA, Santos FLP. Stability analysis and numerical simulations via fractional calculus for tumor dormancy models. *Communications in Nonlinear Science and Numerical Simulation*. 2019; 72: 528-543. Available from: https://doi.org/10.1016/j.cnsns.2019.01.021.

[2] Sotolongo-Costa O, Molina LM, Perez DR, Antoranz J, Reyes MC. Behavior of tumors under nonstationary therapy. *Physica D: Nonlinear Phenomena*. 2003; 178(3-4): 242-253. Available from: https://doi.org/10.1016/S0167-2789(03)00005-8.

[3] Baleanu D, Diethelm K, Scalas E, Trujillo JJ. *Fractional Calculus: Models and Numerical Methods*. 2nd ed. Singapore: World Scientific; 2016. Available from: https://doi.org/10.1142/10044.

[4] Wang KJ. Variational approach for the fractional exothermic reactions model with constant heat source in porous medium. *Thermal Science*. 2023; 27(4): 2879-2885. Available from: https://doi.org/10.2298/TSCI220922211W.

[5] Wang KJ. An effective computational approach to the local fractional low-pass electrical transmission lines model. *Alexandria Engineering Journal*. 2025; 110: 629-635. Available from: https://doi.org/10.1016/j.aej.2024.07.021.

[6] Baleanu D, Mohammadi H, Rezapour S. Analysis of the model of HIV-1 infection of $CD4^{+}$ T-cell with a new approach of fractional derivative. *Advances in Difference Equations*. 2020; 2020: 71. Available from: https://doi.org/10.1186/s13662-020-02544-w.

[7] Murillo-Arcila M, Peris Manguillot A, Vargas Moreno Á. Dynamics of the Caputo fractional derivative. *Fractional Calculus and Applied Analysis*. 2025; 28: 1717-1731. Available from: https://doi.org/10.1007/s13540-025-00430-4.

[8] Alligood KT, Sauer TD, Yorke JA. *Chaos: An Introduction to Dynamical Systems*. 1st ed. New York, NY: Springer; 1996. Available from: https://doi.org/10.1007/b97589.

[9] Kartal N, Kartal S. Complex dynamics of COVID-19 mathematical model on Erdős-Rényi network. *International Journal of Biomathematics*. 2023; 16(5): 2250110. Available from: https://doi.org/10.1142/S1793524522501108.

[10] Gurcan F, Kartal N, Kartal S. Bifurcation and chaos in a fractional-order cournot duopoly game model on scale-free networks. *International Journal of Bifurcation and Chaos*. 2024; 34(8): 2450103. Available from: https://doi.org/10.1142/S0218127424501037.

[11] Kartal N. Multiple bifurcations and chaos control in a coupled network of discrete fractional order predator-prey system. *Iranian Journal of Science*. 2025; 49: 93-106. Available from: https://doi.org/10.1007/s40995-024-01665-1.

[12] Gurcan F, Kartal S. Chaos and its control in a discretized fractional order tumor-immune system model with benign and malignant case. *Journal of Applied Mathematics and Computing*. 2025; 71: 487-515. Available from: https://doi.org/10.1007/s12190-025-02491-3.

[13] Kartal S. A discrete fractional order cournot duopoly game model with relative profit delegation: Stability, bifurcation, chaos, 0-1 testing and control. *Journal of Computational and Applied Mathematics*. 2025; 457: 116284. Available from: https://doi.org/10.1016/j.cam.2024.116284.

[14] Murray JD. *Mathematical Biology: I. An Introduction*. 3rd ed. New York, NY: Springer; 2002. Available from: https://doi.org/10.1007/b98868.
[15] Strogatz SH. *Nonlinear Dynamics and Chaos: With Applications to Physics, Biology, Chemistry, and Engineering*. 2nd ed. Boca Raton: CRC Press; 2015. Available from: https://doi.org/10.1201/9780429492563.
[16] El-Sayed AMA, Salman SM. On a discretization process of fractional-order Riccati differential equation. *Journal of Fractional Calculus and Applications*. 2013; 4(2): 251-259.
[17] Barkat R, Menacer T. Dynamical analysis, stabilization and discretization of a chaotic financial model with fractional order. *Nonlinear Dynamics and Systems Theory*. 2020; 20(3): 253-266.
[18] Agarwal RP, El-Sayed AMA, Salman SM. Fractional-order Chua's system: discretization, bifurcation and chaos. *Advances in Difference Equations*. 2013; 2013(1): 320. Available from: https://doi.org/10.1186/1687-1847-2013-320.
[19] Wiggins S. *Introduction to Applied Nonlinear Dynamical Systems and Chaos*. 1st ed. New York, NY: Springer; 1990. Available from: https://doi.org/10.1007/978-1-4757-4067-7.
[20] Hirsch MW, Smale S, Devaney RL. *Differential Equations, Dynamical Systems, and an Introduction to Chaos*. Waltham, MA: Academic Press; 2013. Available from: https://doi.org/10.1016/C2009-0-61160-0.
[21] Elaydi S. *An Introduction to Difference Equations*. 3rd ed. New York, NY: Springer; 2005. Available from: https://doi.org/10.1007/0-387-27602-5.
[22] Elaydi SN. *Discrete Chaos: With Applications in Science and Engineering*. 2nd ed. New York: Chapman and Hall/CRC; 2007. Available from: https://doi.org/10.1201/9781420011043.
[23] DiStefano JJ, Stubberud AR, Williams IJ. *Schaum's Outline of Theory and Problems of Feedback and Control Systems*. 2nd ed. New York: McGraw-Hill; 2007.
[24] Guckenheimer J, Holmes P. *Nonlinear Oscillations, Dynamical Systems, and Bifurcations of Vector Fields*. 1st ed. New York, NY: Springer; 1983. Available from: https://doi.org/10.1007/978-1-4612-1140-2.
[25] Zhao M, Xuan Z, Li C. Dynamics of a discrete-time predator-prey system. *Advances in Difference Equations*. 2016; 2016(1): 191. Available from: https://doi.org/10.1186/s13662-016-0903-6.
[26] Khan AQ, Qureshi SM, Alotaibi AM. Bifurcation analysis of a three species discrete-time predator-prey model. *Alexandria Engineering Journal*. 2022; 61(10): 7853-7875. Available from: https://doi.org/10.1016/j.aej.2021.12.068.
[27] Din Q, Naseem RA, Shabbir MS. Predator–prey interaction with fear effects: Stability, bifurcation and two-parameter analysis incorporating complex and fractal behavior. *Fractal and Fractional*. 2024; 8(4): 221. Available from: https://doi.org/10.3390/fractalfract8040221.
[28] Chen G, Dong X. *From Chaos to Order: Methodologies, Perspectives and Applications*. Singapore: World Scientific; 1998. Available from: https://doi.org/10.1142/3033.
[29] Lin Y, Din Q, Rafaqat M, Elsadany AA, Zeng Y. Dynamics and chaos control for a discrete-time Lotka–Volterra model. *IEEE Access*. 2020; 8: 126760-126775. Available from: https://doi.org/10.1109/ACCESS.2020.3008522.
[30] de Pillis LG, Fister KR, Gu W, Head T, Maples K, Neal T, et al. Optimal control of mixed immunotherapy and chemotherapy of tumors. *Journal of Biological Systems*. 2008; 16(1): 51-80. Available from: https://doi.org/10.1142/S0218339008002435.
[31] de Pillis LG, Gu W, Radunskaya AE. Mixed immunotherapy and chemotherapy of tumors: Modeling, applications and biological interpretations. *Journal of Theoretical Biology*. 2006; 238(4): 841-862. Available from: https://doi.org/10.1016/j.jtbi.2005.06.037.
[32] Rosenberg SA. IL-2: the first effective immunotherapy for human cancer. *The Journal of Immunology*. 2014; 192(12): 5451-5458. Available from: https://doi.org/10.4049/jimmunol.1490019.
[33] Foo J, Leder K. Dynamics of cancer recurrence. *The Annals of Applied Probability*. 2013; 23(4): 1437-1468. Available from: https://doi.org/10.1214/12-AAP876.
[34] de Pillis LG, Radunskaya AE, Wiseman CL. A validated mathematical model of cell-mediated immune response to tumor growth. *Cancer Research*. 2005; 65(17): 7950-7958. Available from: https://doi.org/10.1158/0008-5472.CAN-05-0564.
[35] Rodríguez-Pérez D, Sotolongo-Grau O, Espinosa Riquelme R, Sotolongo-Costa O, Santos Miranda JA, Antoranz JC. Assessment of cancer immunotherapy outcome in terms of the immune response time features. *Mathematical Medicine and Biology: A Journal of the IMA*. 2007; 24(3): 287-300. Available from: https://doi.org/10.1093/imammb/dqm003.

[36] Sandri M. Numerical calculation of Lyapunov exponents. *The Mathematica Journal*. 1996; 6(3): 78-84.

[37] Wolf A, Swift JB, Swinney HL, Vastano JA. Determining Lyapunov exponents from a time series. *Physica D: Nonlinear Phenomena*. 1985; 16(3): 285-317. Available from: https://doi.org/10.1016/0167-2789(85)90011-9.

[38] Zheng D, Preuss K, Milano MT, He X, Gou L, Shi Y, et al. Mathematical modeling in radiotherapy for cancer: A comprehensive narrative review. *Radiation Oncology*. 2025; 20: 49. Available from: https://doi.org/10.1186/s13014-025-02626-7.

[39] Azizi T. Mathematical modelling of cancer treatments, resistance, optimization. *Applied Mathematics*. 2025; 5(2): 40. Available from: https://doi.org/10.3390/appliedmath5020040.

[40] Kuznetsov YA. *Elements of Applied Bifurcation Theory*. 4th ed. Cham, Switzerland: Springer Cham; 2023. Available from: https://doi.org/10.1007/978-3-031-22007-4.

Appendix A

A.1 *nondimensionalization steps*

The main model studied in this paper was first introduced by Sotolongo-Costa et al. [2], who modified the classical predator-prey model to describe the interactions between tumor cells and lymphocytes. The model is given by

$$\begin{aligned} \frac{dX}{dt} &= aX - bXY, \\ \frac{dY}{dt} &= u - fY - KX + dXY, \end{aligned} \tag{21}$$

where $X(t)$ is the population of tumor cells, and $Y(t)$ is the population of lymphocytes.

According to Sotolongo-Costa et al. [2], system (21) was first written in dimensional form and later transformed into a nondimensional form by rescaling the dimensional variables $X(t)$, $Y(t)$, and t. The transformation was done to simplify the analysis by converting the dimensional variables $X(t)$, $Y(t)$, and t into the nondimensional variables $x(\tau)$, $y(\tau)$, and τ, and to reduce the number of parameters that control the dynamics [14].

Following Sotolongo-Costa et al. [2], the transformation steps are given below. First, we introduce the scaled variables

$$X = x\,X_s,\ \ Y = y\,Y_s,\ \ \text{and}\ t = \ \tau\,T_s,$$

where X_s, Y_s, and T_s are the scaling factors. Since $\tau = \dfrac{t}{T_s}$, it follows that $\dfrac{d\tau}{dt} = \dfrac{1}{T_s}$.

By the chain rule, we therefore have

$$\frac{d}{dt} = \frac{d\tau}{dt} \cdot \frac{d}{d\tau} = \frac{1}{T_s}\frac{d}{d\tau}.$$

For $X = x\,X_s$, we have

$$\frac{dX}{dt} = \frac{d(x\,X_s)}{dt} = \frac{X_s}{T_s}\,\frac{dx}{d\tau}. \tag{22}$$

Similarly, for $Y = y\,Y_s$,

$$\frac{dY}{dt} = \frac{Y_s}{T_s}\,\frac{dy}{d\tau}. \tag{23}$$

Now, by substituting equations (22) and (23) into system (21) , we have

$$\frac{X_s}{T_s}\frac{dx}{d\tau} = a(xX_s) - b(xX_syY_s),$$

$$\frac{Y_s}{T_s}\frac{dy}{d\tau} = u - f(yY_s) - K(xX_s) + d(xX_s yY_s). \tag{24}$$

Next, by simplifying both sides of system (24), we get

$$\begin{aligned} \frac{dx}{d\tau} &= T_s\left(ax - bxyY_s\right), \\ \frac{dy}{d\tau} &= T_s\left(\frac{u}{Y_s} - fy - K(x\,\frac{X_s}{Y_s}) + d(xyX_s)\right), \end{aligned} \tag{25}$$

substituting $T_s = \dfrac{1}{\sqrt{af}}$, $X_s = \dfrac{\sqrt{af}}{d}$, and $Y_s = \dfrac{\sqrt{af}}{b}$ to system (25), we obtain the nondimentional model

$$\frac{dx}{d\tau} = \rho x - xy,$$

$$\frac{dy}{d\tau} = \sigma - \frac{1}{\rho}y - kx + xy,$$

where $\rho = \sqrt{\dfrac{a}{f}}$, $\sigma = \dfrac{ub}{af}$, and $k = \dfrac{Kb}{d\sqrt{af}}$.

A.2 *Computation of β and γ*

Below are the steps for obtaining β and γ for Lemma 1 (iii).
Assuming that a center manifold has the form $Y = h(X) = \beta X^2 + \gamma X^3 + \mathcal{O}(|X|^4)$ then, it must satisfy

$$h(X + \frac{h^\alpha}{\Gamma(1+\alpha)}f(X, h(X)) = \left(1 - \frac{h^\alpha}{r\Gamma(1+\alpha)}\right)h(X) + \frac{h^\alpha}{\Gamma(1+\alpha)}g(X, h(X)).$$

Thus,

$$\beta(X + \frac{h^\alpha}{\Gamma(1+\alpha)}(-rX^2(r-d) - X(\beta X^2 + \gamma X^3 + \mathcal{O}(|X|^4))))^2 + \gamma(X + \ldots)^3 = R, \tag{26}$$

where

$$R = \left(1 - \frac{h^\alpha}{r\Gamma(1+\alpha)}\right)(\beta X^2 + \gamma X^3 + \mathcal{O}(|X|^4))$$

$$+ \frac{h^\alpha}{\Gamma(1+\alpha)}\left(rX^2(r-d)\left(-dr + r^2 + 1\right)\right)$$

$$+X(\beta X^2+\gamma X^3+\mathcal{O}(|X|^4))\left(-dr+r^2+1\right). \tag{27}$$

Now, from equations (26) and (27), we obtain

$$X^2\colon \beta=\beta\left(1-\frac{h^\alpha}{r\Gamma(1+\alpha)}\right)+\frac{h^\alpha}{\Gamma(1+\alpha)}\left(r(r-d)\left(-dr+r^2+1\right)\right), \tag{28}$$

$$X^3\colon 2\beta\frac{h^\alpha}{\Gamma(1+\alpha)}(rd-r^2)+\gamma=\gamma\left(1-\frac{h^\alpha}{r\Gamma(1+\alpha)}\right)+\beta\frac{h^\alpha}{\Gamma(1+\alpha)}(1-rd+r^2), \tag{29}$$

solving (28) for β, we obtain

$$\beta=r(r^2-rd)\left(-dr+r^2+1\right).$$

Now, substituting $\beta=r(r^2-rd)(1-rd+r^2)$ into equation (29), we obtain

$$\gamma=r^2(r^2-rd)(1-rd+r^2)(3r^2-3rd+1).$$

A.3 *Derivation of σ**

Among the three boundary values of σ obtained from the stability conditions in Theorem (2), the value $\sigma^*=\dfrac{1}{\dfrac{r}{d-r}-\dfrac{rh^\alpha}{\Gamma(1+\alpha)}}+1$ is the only for which the eigenvalues of the Jacobian matrix (8) form a complex conjugates pair with modulus 1. Therefore, a Neimark-Sacker bifurcation is expected to occur [22].

A.4 *Transformation matrix T*

Let

$$D=\begin{pmatrix} 1 & -\dfrac{h^\alpha}{r\left(\Gamma(1+\alpha)+(r-d)h^\alpha\right)} \\ -\dfrac{(d-r)h^\alpha}{\Gamma(1+\alpha)} & \dfrac{(d-r)h^{2\alpha}}{r\Gamma(1+\alpha)(r-d)h^\alpha+r\Gamma(1+\alpha)^2}+1 \end{pmatrix},$$

and its eigenvalues are

$$\lambda_{1,2}=\frac{dh^{2\alpha}-2dr\Gamma(1+\alpha)h^\alpha-rh^{2\alpha}+2r^2\Gamma(1+\alpha)h^\alpha+2r\Gamma(1+\alpha)^2}{2r\Gamma(1+\alpha)\left(\Gamma(1+\alpha)-dh^\alpha+rh^\alpha\right)}$$

$$\pm\frac{h^\alpha\sqrt{d-r}\sqrt{dh^{2\alpha}-4dr\Gamma(1+\alpha)h^\alpha-rh^{2\alpha}+4r^2\Gamma(1+\alpha)h^\alpha+4r\Gamma(1+\alpha)^2}}{2r\Gamma(1+\alpha)\left(\Gamma(1+\alpha)-dh^\alpha+rh^\alpha\right)}$$

$$= a \pm ib$$

and the eigenvectors associated with the eigenvalues are

$$v_1 = \begin{pmatrix} \dfrac{rh^\alpha - dh^\alpha + \sqrt{-(r-d)(dh^{2\alpha} - 4dr\Gamma(1+\alpha)h^\alpha - rh^{2\alpha} + 4r^2\Gamma(1+\alpha)h^\alpha + 4r\Gamma(1+\alpha)^2)}}{2r(d-r)\left(-\Gamma(1+\alpha) + dh^\alpha - rh^\alpha\right)} \\ 1 \end{pmatrix},$$

and

$$v_2 = \begin{pmatrix} \dfrac{rh^\alpha - dh^\alpha - \sqrt{-(r-d)(dh^{2\alpha} - 4dr\Gamma(1+\alpha)h^\alpha - rh^{2\alpha} + 4r^2\Gamma(1+\alpha)h^\alpha + 4r\Gamma(1+\alpha)^2)}}{2r(d-r)\left(-\Gamma(1+\alpha) + dh^\alpha - rh^\alpha\right)} \\ 1 \end{pmatrix},$$

respectively. Since the eigenvalues are complex conjugates, the columns of the transformation matrix T are formed from the real and imaginary parts of the eigenvector v_1 (or equivalently v_2, since they are conjugates) [20].

A.5 *Computation details for equation (16)*

By applying the translation $\begin{pmatrix} u \\ v \end{pmatrix} = T \begin{pmatrix} X \\ Y \end{pmatrix}$, we have

$$T \begin{pmatrix} X \\ Y \end{pmatrix} \to DT \begin{pmatrix} X \\ Y \end{pmatrix} + \begin{pmatrix} -\dfrac{uvh^\alpha}{\Gamma(1+\alpha)} \\ \\ \dfrac{uvh^\alpha}{\Gamma(1+\alpha)} \end{pmatrix}, \tag{30}$$

where

$$u = -\frac{\sqrt{(r-d)\left(dh^{2\alpha} - 4dr\Gamma(1+\alpha)h^\alpha - rh^{2\alpha} + 4r^2\Gamma(1+\alpha)h^\alpha + 4r\Gamma(1+\alpha)^2\right)}}{2r(d-r)\left(-\Gamma(1+\alpha) + dh^\alpha - rh^\alpha\right)} X$$

$$+ \frac{rh^\alpha - dh^\alpha}{2r(d-r)\left(-\Gamma(1+\alpha) + dh^\alpha - rh^\alpha\right)} Y,$$

$$v = Y.$$

Applying T^{-1} to both sides of (30) gives

$$\begin{pmatrix} X \\ Y \end{pmatrix} \to T^{-1}DT \begin{pmatrix} X \\ Y \end{pmatrix} + T^{-1} \begin{pmatrix} -\dfrac{uvh^{\alpha}}{\Gamma(1+\alpha)} \\ \\ \dfrac{uvh^{\alpha}}{\Gamma(1+\alpha)} \end{pmatrix},$$

which simplifies to

$$\begin{pmatrix} X \\ Y \end{pmatrix} \to \begin{pmatrix} a & -b \\ \\ b & a \end{pmatrix} \begin{pmatrix} X \\ Y \end{pmatrix} + \begin{pmatrix} F_1(X,Y) \\ \\ F_2(X,Y) \end{pmatrix}.$$

A.6 *Computational details for k*

This Appendix summarizes the main steps of computing the coefficient k mentioned in Theorem 3, where k plays an important role in determining the stability of the invariant circle. If $k<0$, then the invariant closed curve is asymptotically stable. Hence, a supercritical Neimark-Sacker bifurcation occurs. In contrast, if $k>0$, then the invariant closed curve is unstable. Hence, a subcritical Neimark-Sacker bifurcation occurs [40].

We have

$$F_1(X,Y) = -\frac{X\,Y\,h^{\alpha}\left(\left(-2dr+2r^2+1\right)h^{\alpha}+2r\Gamma(1+\alpha)\right)}{2r\Gamma(1+\alpha)\left(\Gamma(1+\alpha)+(r-d)h^{\alpha}\right)}$$

$$-\frac{Y^2\,h^{\alpha}\left(dh^{\alpha}-rh^{\alpha}\right)\left(\left(-2dr+2r^2+1\right)h^{\alpha}+2r\Gamma(1+\alpha)\right)}{2r\Gamma(1+\alpha)\left(\Gamma(1+\alpha)+(r-d)h^{\alpha}\right)\sqrt{(d-r)\left((r-d)h^{2\alpha}+4r\Gamma(1+\alpha)(d-r)h^{\alpha}-4r\Gamma(1+\alpha)^2\right)}},$$

$$F_2(X,Y) = -\frac{h^{\alpha}\left(dh^{\alpha}-rh^{\alpha}\right)}{2r\Gamma(1+\alpha)(d-r)\left((d-r)h^{\alpha}-\Gamma(1+\alpha)\right)}Y^2$$

$$-\frac{h^{\alpha}\sqrt{(d-r)\left((r-d)h^{2\alpha}+4r\Gamma(1+\alpha)(d-r)h^{\alpha}-4r\Gamma(1+\alpha)^2\right)}}{2r\Gamma(1+\alpha)(d-r)\left((d-r)h^{\alpha}-\Gamma(1+\alpha)\right)}X\,Y.$$

Evaluating the partial derivative of $F_1(X,Y)$, and $F_2(X,Y)$ to compute the coefficient k, we have

$$F_{1X} = -\frac{Yh^{\alpha}\left(\left(-2dr+2r^2+1\right)h^{\alpha}+2r\Gamma(1+\alpha)\right)}{2r\Gamma(1+\alpha)\left(\Gamma(1+\alpha)+(r-d)h^{\alpha}\right)}$$

$$F_{1XX} = F_{1XXX} = 0$$

$$F_{1Y} = -\frac{Xh^{\alpha}\left(\left(-2dr+2r^2+1\right)h^{\alpha}+2r\Gamma(1+\alpha)\right)}{2r\Gamma(1+\alpha)\left(\Gamma(1+\alpha)+(r-d)h^{\alpha}\right)}$$

$$-\frac{Yh^{\alpha}\left(dh^{\alpha}-rh^{\alpha}\right)\left(\left(-2dr+2r^{2}+1\right)h^{\alpha}+2r\Gamma(1+\alpha)\right)}{r\Gamma(1+\alpha)\left(\Gamma(1+\alpha)+(r-d)h^{\alpha}\right)\sqrt{(d-r)\left((r-d)h^{2\alpha}+4r\Gamma(1+\alpha)(d-r)h^{\alpha}-4r\Gamma(1+\alpha)^{2}\right)}}$$

$$F_{1YY}=-\frac{h^{\alpha}\left(dh^{\alpha}-rh^{\alpha}\right)\left(\left(-2dr+2r^{2}+1\right)h^{\alpha}+2r\Gamma(1+\alpha)\right)}{r\Gamma(1+\alpha)\left(\Gamma(1+\alpha)+(r-d)h^{\alpha}\right)\sqrt{(d-r)\left((r-d)h^{2\alpha}+4r\Gamma(1+\alpha)(d-r)h^{\alpha}-4r\Gamma(1+\alpha)^{2}\right)}}$$

$$F_{1YYY}=0$$

$$F_{1XY}=-\frac{h^{\alpha}\left(\left(-2dr+2r^{2}+1\right)h^{\alpha}+2r\Gamma(1+\alpha)\right)}{2r\Gamma(1+\alpha)\left(\Gamma(1+\alpha)+(r-d)h^{\alpha}\right)}$$

$$F_{1XYY}=0$$

$$F_{1XXY}=0$$

$$F_{2X}=-\frac{Yh^{\alpha}\sqrt{(d-r)\left((r-d)h^{2\alpha}+4r\Gamma(1+\alpha)(d-r)h^{\alpha}-4r\Gamma(1+\alpha)^{2}\right)}}{2r\Gamma(1+\alpha)(d-r)\left((d-r)h^{\alpha}-\Gamma(1+\alpha)\right)}$$

$$F_{2XX}=F_{2XXX}=0$$

$$F_{2Y}=-\frac{Yh^{\alpha}\left(dh^{\alpha}-rh^{\alpha}\right)}{r\Gamma(1+\alpha)(d-r)\left((d-r)h^{\alpha}-\Gamma(1+\alpha)\right)}-\frac{Xh^{\alpha}\sqrt{(d-r)\left((r-d)h^{2\alpha}+4r\Gamma(1+\alpha)(d-r)h^{\alpha}-4r\Gamma(1+\alpha)^{2}\right)}}{2r\Gamma(1+\alpha)(d-r)\left((d-r)h^{\alpha}-\Gamma(1+\alpha)\right)}$$

$$F_{2YY}=-\frac{h^{\alpha}\left(dh^{\alpha}-rh^{\alpha}\right)}{r\Gamma(1+\alpha)(d-r)\left((d-r)h^{\alpha}-\Gamma(1+\alpha)\right)}$$

$$F_{2YYY}=0$$

$$F_{2XY}=-\frac{h^{\alpha}\sqrt{(d-r)\left((r-d)h^{2\alpha}+4r\Gamma(1+\alpha)(d-r)h^{\alpha}-4r\Gamma(1+\alpha)^{2}\right)}}{2r\Gamma(1+\alpha)(d-r)\left((d-r)h^{\alpha}-\Gamma(1+\alpha)\right)}$$

$$F_{2XYY}=0$$

$$F_{2XXY}=0$$

Now, since the partial derivatives are calculated, then ξ_{20}, ξ_{11}, ξ_{02}, and ξ_{21} can be computed as

$$\xi_{20}=\frac{1}{8}\left(\frac{2h^{\alpha}\left((d-r)h^{\alpha}-2\Gamma(1+\alpha)\right)}{\Gamma(1+\alpha)\sqrt{(r-d)\left((d-r)h^{2\alpha}+4r\Gamma(1+\alpha)\left(\Gamma(1+\alpha)+(r-d)h^{\alpha}\right)\right)}}+i\,\frac{2h^{\alpha}}{\Gamma(1+\alpha)}\right)$$

$$\xi_{11} = \frac{1}{4}\left(\frac{(r-d)h^{2\alpha}\left((2r(r-d)+1)h^{\alpha}+2r\Gamma(1+\alpha)\right)}{r\Gamma(1+\alpha)\left(\Gamma(1+\alpha)+(r-d)h^{\alpha}\right)\sqrt{(d-r)\left((r-d)h^{2\alpha}-4r\Gamma(1+\alpha)\left(\Gamma(1+\alpha)+(r-d)h^{\alpha}\right)\right)}} \right.$$

$$\left. + i\frac{h^{2\alpha}}{r\Gamma(1+\alpha)(r-d)h^{\alpha}+r\Gamma(1+\alpha)^2} \right)$$

$$\xi_{02} = \frac{1}{8}\left(\frac{2r\Gamma(1+\alpha)h^{\alpha}\left(2\Gamma(1+\alpha)+(r-d)h^{\alpha}\right)-2(d-r)(r(d-r)-1)h^{3\alpha}}{r\Gamma(1+\alpha)\left(\Gamma(1+\alpha)+(r-d)h^{\alpha}\right)\sqrt{(d-r)\left((r-d)h^{2\alpha}-4r\Gamma(1+\alpha)\left(\Gamma(1+\alpha)+(r-d)h^{\alpha}\right)\right)}} \right.$$

$$\left. + i\,\frac{2}{\Gamma(1+\alpha)\left(\frac{1}{(-dr+r^2+1)h^{\alpha}+r\Gamma(1+\alpha)}-h^{-\alpha}\right)} \right)$$

$$\xi_{21} = 0$$

Thus, a complex calculation yields

$$k = \frac{n_1}{8r^3\Gamma(1+\alpha)^3\left(\Gamma(1+\alpha)+(r-d)h^{\alpha}\right)^3},$$

where

$$n_1 = h^{2\alpha}\Big[(d-r)(-dr+r^2+1)^2h^{4\alpha}+r\Gamma(1+\alpha)\Big(\big((d-r)(r(d-r)-2)(r(d-r)-1)h^{3\alpha}$$

$$+ r\Gamma(1+\alpha)\big(-3(r-d)(-dr+r^2+1)h^{2\alpha}+\Gamma(1+\alpha)(3r(d-r)-1)h^{\alpha}-r\Gamma(1+\alpha)^2\big)\Big)\Big].$$